Origins and Dynamics of the 90-Day and 30–60-Day Variations in the Equatorial Indian Ocean

WEIQING HAN

Program in Atmospheric and Oceanic Sciences, University of Colorado, Boulder, Colorado

(Manuscript received 6 March 2004, in final form 13 September 2004)

ABSTRACT

Sea level observations in the equatorial Indian Ocean show a dominant spectral peak at 90 days and secondary peaks at 30–60 days over an intraseasonal period (20–90 days). A detailed investigation of the origins and dynamics of these variations is carried out using an ocean general circulation model, namely, the Hybrid Coordinate Ocean Model (HYCOM). Two parallel experiments are performed in the tropical Indian Ocean basin for the period 1988–2001: one is forced by NCEP 3-day mean forcing fields together with the Climate Prediction Center (CPC) Merged Analysis of Precipitation (CMAP) pentad precipitation, and the other is forced by monthly mean fields. To help to understand the role played by the wind-driven equatorial wave dynamics, a linear continuously stratified ocean model is also used. Both the observed and modeled 90-day sea level anomaly fields and HYCOM surface current clearly show equatorial Kelvin and first-meridional-mode Rossby wave structures that are forced by the 90-day winds. The wind amplitude at the 90-day period, however, is weaker than that for the 30–60-day period, suggesting that the equatorial Indian Ocean selectively responds to the 90-day winds. This selective response arises mainly from the resonant excitation of the second-baroclinic-mode ($n = 2$) waves by the 90-day winds. In this case, Rossby waves reflected from the eastern ocean boundary enhance the directly forced response in the ocean interior, strengthening the 90-day peak. In addition, the directly forced response increases monotonically with the increase of forcing period, contributing to the larger variances of currents and sea level at 90 days. Two factors account for this monotonic increase in directly forced response. First, at lower frequency, both Rossby and Kelvin waves associated with the low-order baroclinic modes have longer wavelengths, which are more efficiently excited by the larger-scale winds. Second, responses of the high-order modes directly follow the local winds, and their amplitudes are proportional to both forcing period and wind strength. Although most energy is surface trapped, there is a significant amount that propagates through the pycnocline into the deep ocean. The dominance of the 90-day peak occurs not only at the surface but also in the deeper layers down to 600 m. In the deeper ocean, both the directly forced response and reflected waves associated with the first two baroclinic modes contribute to the 90-day variation. Spectra of the observed sea surface temperature (SST) also show a 90-day peak, likely a result of the selective response of the equatorial Indian Ocean at the 90-day period. Near the surface, the spectral peaks of currents and sea level at the 30–60-day period are directly forced by winds that peak at 30–60 days. In the deeper layers, both directly forced and reflected waves associated with the first two baroclinic modes contribute. Oceanic instabilities can have significant contributions only near the western boundary and near 5°N south of Sri Lanka.

1. Introduction

a. Observations

Sea level observations in the equatorial Indian Ocean show a primary spectral peak at 90 days and secondary peaks at 30–60 days over the intraseasonal band (20–90-day period; Fig. 1). Particularly, the 90-day spectral peak of the sea level anomaly (SLA) exhibits distinct spatial structures, with double maxima occurring at 4°–5°N and 4°–5°S about the equator in the central basin (Figs. 1a, b) and a single maximum near the equator in the eastern basin (Fig. 1c). These spectral peaks also appear in 8-yr (1992–99) daily sea level station data near the Gan Island (0°41′S, 73°09′E), which shows a maximum spectral peak near 90 days and a secondary peak near 48 days with both peaks above 95% significance (Fig. 2). The 90-day sea level oscillation in the equatorial Indian Ocean was also shown by Schouten et al. (2002).

In the far-eastern Indian Ocean near the Indonesian Seas, a strong 90-day peak of sea level was observed in tide-gauge data during 1988–90 at Benoa (8.7°S, 115.2°E) and during 1991–93 at Christmas Island

Corresponding author address: Dr. Weiqing Han, PAOS, University of Colorado, Campus Box 311, Boulder, CO 80309.
E-mail: whan@enso.colorado.edu

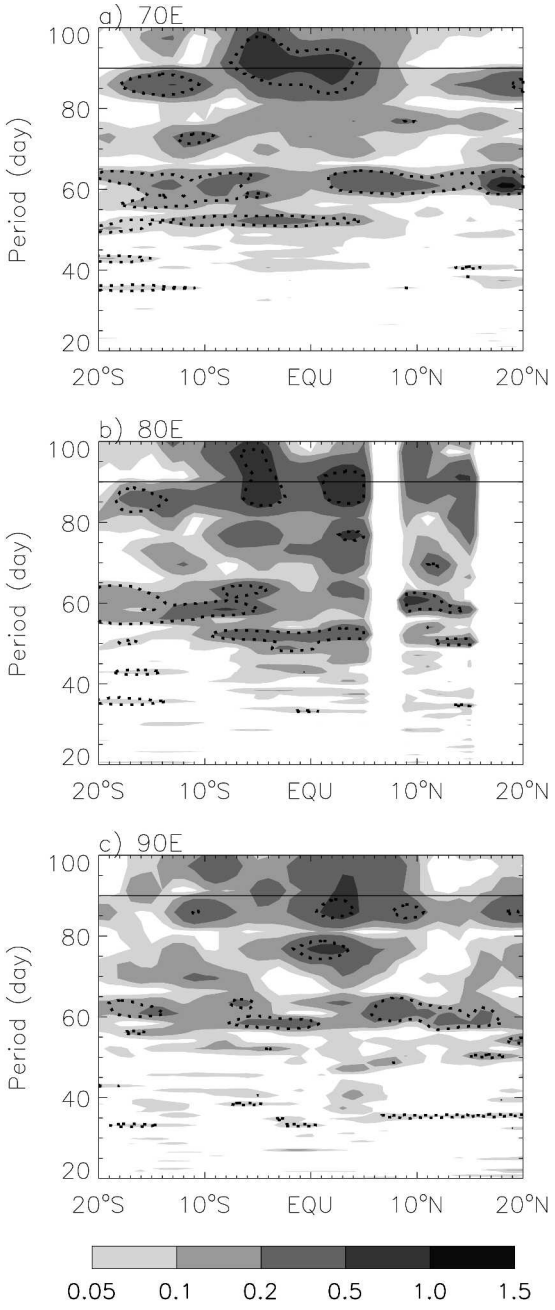

FIG. 1. Meridional section for variance spectra (cm^2) of TOPEX/Poseidon SLA along (a) 70°, (b) 80°, and (c) 90°E, based on an 8-yr record (1993–2000) with a 10-day resolution. Dashed contours are the 95% significance level. The 90-day and most 30–60-day spectral peaks are above 95% significance.

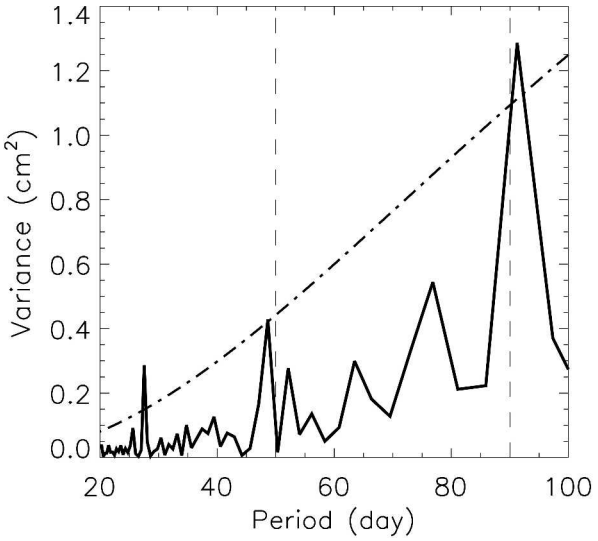

FIG. 2. Variance spectra (cm^2) for daily sea level station data at Gan (0°41′S, 73°09′E) based on the record of 1992–99 with dash–dotted curve representing 95% significance level. The data were downloaded from the University of Hawaii Data Center.

(10.4°S, 105.7°E; Qiu et al. 1999). Near the Timor Passage, the observed along channel flow at (11.3°S, 122.9°E) during 1992 showed spectral peaks near 80–90- and 30–60-day periods (Qiu et al. 1999).

While the 90-day variation has been discovered rather recently, the 30–60-day currents were detected at several locations of the equatorial Indian Ocean by earlier studies. In the western equatorial basin at (47°–62°E), the moored current meter data during April 1979–June 1980 showed a spectral peak of zonal current at 30–60 days at 200 m (Luyten and Roemmich 1982). Mertz and Mysak (1984) reported a 40–50-day oscillation of the longshore current between 0° and 5°S of the western Indian Ocean, suggesting that winds associated with the Madden–Julian oscillation (MJO; Madden and Julian 1971, 1972) in the western equatorial region were the forcing.

In the central basin near the Gan Island (0°41′S, 73°10′E), a 2.5-yr, weekly sampled data record during January 1973–May 1975 was analyzed by McPhaden (1982). He found zonal wind to be highly coherent with the zonal currents, mixed layer depth, and upper-thermocline temperature at period of 30–60 days. Near 80°E, measurements from a current meter mooring deployed along 80°30′E between 45′S and 5°N during July 1993–September 1994 as part of the World Ocean Circulation Experiment (WOCE) showed a relative energy peak at 40–60 days for the zonal, near-surface equatorial currents (Reppin et al. 1999; Schott and McCreary 2001).

b. Theoretical background

Using both linear and nonlinear versions of a 4½-layer ocean model, Han et al. (2001a) examined the dynamics of the intraseasonal zonal currents along the equatorial Indian Ocean. Their solutions revealed that the dominant spectral peak of intraseasonal currents occurs at 90 days and there are secondary peaks at 30–60 days. Given that their model only had four ver-

tical degrees of freedom, Han et al. (2001a) focused on discussing surface current features. They attributed the 90-day current to the preferential excitation of Kelvin and Rossby waves by the larger-scale, lower-frequency 90-day winds, and to enhancement by Rossby waves reflected from the eastern ocean boundary. They also concluded that the relative spectral peak at the 30–60-day period results primarily from direct wind forcing, and that the contribution from reflected waves is negligible.

Qiu et al. (1999) examined the forcing mechanisms of intraseasonal currents in the far-eastern Indian Ocean near the Indonesian Seas using a 1½-layer ocean model. They suggested that the observed 80–90- and 30–60-day spectral peaks in current and sea level are remotely forced by winds in the central equatorial Indian Ocean.

In fact, the origin of 30–60-day currents in the equatorial Indian Ocean have been investigated in several earlier modeling studies. Moore and McCreary (1990) used a linear, continuously stratified model to demonstrate that the observed 40–50-day current in the western Indian Ocean was forced by the 40–50-day winds associated with the MJO. Kindle and Thompson (1989) forced their 1½-layer, reduced-gravity ocean model by monthly mean winds, and yet still obtained a 40–50-day oscillation that originated in the western Indian Ocean; they suggested that it was generated by barotropic instability associated with the East African Coastal Current beginning around April of each year. The 50-day unstable waves also appeared in results from the Woodbury et al. (1989) reduced-gravity model forced by monthly mean winds. Sengupta et al. (2001) forced an ocean general circulation model (OGCM) with daily National Centers for Environmental Prediction (NCEP) wind stress, and obtained 30–50-day fluctuations located in the western equatorial regime and in the central equatorial region around Sri Lanka. They concluded that oceanic instabilities play an important role in causing these fluctuations.

Although the 90-day spectral peak of zonal surface current was discussed by Han et al. (2001a), the spatial structure, vertical penetration, and generation of the 90-day variation as a whole have not been examined. The possibility that the 90-day oscillation has a coupled nature has not been demonstrated. Although the dynamics of the 30–60-day near-surface currents in the equatorial Indian Ocean have been discussed in previous studies, their subsurface variabilities have not been investigated. The relative importance of intraseasonal winds and oceanic instabilities has never been quantified.

c. Present research

The goal of this study is to provide a detailed understanding of the origins and dynamics of the 90- and 30–60-day variations in the equatorial Indian Ocean. For this purpose, an OGCM—the Hybrid Coordinate Ocean Model (HYCOM)—is used as a primary tool. To help understand the role played by the wind-driven equatorial wave dynamics, a linear, continuously stratified ocean model (LM) is also used.

Atmospheric intraseasonal variabilities generated in the equatorial Indian Ocean can propagate poleward, causing active and break phases of the Asian–Australian monsoon, as well as eastward into the Pacific to affect ENSO. Thus a detailed understanding of how the equatorial Indian Ocean responds to the atmospheric intraseasonal variability, and how the oceanic response feeds back onto the atmosphere, is an important step toward understanding their impacts on monsoon and ENSO. Additionally, since intraseasonal atmospheric forcing can cause a significant seasonal-to-interannual rectification in zonal current and transport in the equatorial Indian Ocean (Waliser et al. 2003; Han et al. 2004), this study will potentially contribute to our understanding of climate variability and predictability in general.

2. The ocean models

a. HYCOM

Since HYCOM is documented in detail elsewhere (see Bleck 2002), here only a brief description of aspects relevant to this paper is provided. HYCOM has a hybrid vertical coordinate, which is isopycnal in the open, stratified ocean, but smoothly reverts to a terrain-following coordinate in shallow coastal regions, and to z-level coordinates in the mixed layer and/or unstratified seas. It is intended to integrate the advantages of isopycnic, z-level, and terrain-following coordinates, and thus can retain its water-mass characteristics for centuries, have high vertical resolution in the surface mixed layer, maintain sufficient vertical resolution in unstratified or weakly stratified regions of the ocean, and have high vertical resolution in coastal regions. The feasibility of the hybrid coordinate approach for handling both deep and shallow regions throughout the annual heating/cooling cycle has been demonstrated for the North Atlantic by Halliwell (1998, 2004).

1) Indian Ocean configuration

In this paper, HYCOM is configured to the tropical Indian Ocean north of 30°S, with a horizontal resolution of $0.5° \times 0.5°$ and a realistic bottom topography. Vertically, 18 sigma layers are chosen with a fine resolution in the upper ocean to better resolve the vertical structures of upper-ocean currents, temperature, mixed layer, and thermocline. Reference pressure sigma-0 is adopted, because our focus is on upper-ocean processes. The nonlocal K-profile parameterization (KPP) is used for the boundary layer mixing scheme (Large et al. 1994, 1997). Solar shortwave radiation penetration is included with Jerlov water type IA (Jerlov 1976).

Along the continental boundaries, no-slip boundary conditions are applied. Near the southern boundary, a sponge layer of 5° (25°–30°S) is applied to relax the model temperature and salinity to the Levitus and Boyer (1994) and Levitus et al. (1994) climatologies. Lateral boundary forcing due to the Indonesian Throughflow is included by relaxing the model temperature and salinity to Levitus data in the Throughflow region. Freshwater due to the Bay of Bengal rivers is neglected, as only a small portion of the river water reaches the equator, and its effect on currents and SST are negligible in the equatorial region (Han et al. 2001b; Howden and Murtugudde 2001). Bottom topographic data are from the ETOPO5 smoothed over a 10° × 10° bin.

2) FORCING AND SPINUP

The wind stress, wind speed, air temperature, specific humidity, solar shortwave radiation, and outgoing longwave radiation used to force HYCOM are from the NCEP–National Center for Atmospheric Research (NCAR) reanalysis for the period 1988–2001 (Kalnay et al. 1996). This period of time is chosen because it includes the periods of WOCE current measurement and Ocean Topography Experiment (TOPEX)/Poseidon altimeter data. At the same time, it is sufficiently long for documenting the 90-day currents with statistic significance. Two versions of these forcing fields are utilized: 3-day mean, which includes intraseasonal variabilities, and monthly mean, which excludes them. Precipitation is from the Climate Prediction Center (CPC) Merged Analysis of Precipitation (CMAP) pentad and monthly mean rainfall data for the same period of time (Xie and Arkin 1996). The pentad precipitation is interpolated onto the 3-day resolution that corresponds to the 3-day NCEP data.

The model is spun up from a state of rest for 20 yr using the Comprehensive Ocean–Atmosphere Data Set (COADS) monthly mean climatological fields. Based on the results of year 20, HYCOM is integrated forward in time using the 3-day and monthly forcing fields for the period of 1988–2001. Results for years 1990–2001 are analyzed.

b. The LM

The linear, continuously stratified ocean model is described in detail by McCreary (1980, 1981), and it has been applied to several Indian Ocean studies (Shankar et al. 1996; McCreary et al. 1996; Miyama et al. 2003; Han et al. 2004). The equations of motion are linearized about a state of rest with a realistic background stratification, and the ocean bottom is assumed flat. With these restrictions, solutions can be represented as expansions in the vertical normal modes of the system, and the total solution is the sum of all the modes. In this paper, the first 25 baroclinic modes are used and solutions are well converged. The characteristic speeds c_n for the first few modes estimated from buoyancy frequency N_b based on Indian Ocean density observation (see Moore and McCreary 1990) are $c_1 = 264$ cm s^{-1}, $c_2 = 167$ cm s^{-1}, $c_3 = 105$ cm s^{-1}, and $c_4 = 75$ cm s^{-1}.

TABLE 1. OGCM and LM experiments. See text for detailed description.

Expt	Forcing	Duration
OGCM_MR	3-day mean	1988–2001
OGCM_BR	Monthly mean	1988–2001
LM_MR	3-day winds, no Maldives	1988–2001
LM_FR	Same as LM_MR but with damper	1988–2001
LMMD_MR	Same as LM_MR but with Maldives	1988–2001

The model basin is the same realistic Indian Ocean north of 30°S as used in HYCOM. The grid resolution is $\Delta x = \Delta y = 55$ km, close to the 0.5° × 0.5° HYCOM grid. The Maldives Islands are represented by rectangular boxes along 73–74°E at 0°–1°N and 2°–6°N. Along the continental and island boundaries, no-slip boundary conditions are used. The southern boundary is open, and zero-gradient boundary conditions are applied. The linear model is first spun up for 20 yr using the monthly climatology of COADS wind stress forcing. Restarting from year 20, the model is integrated forward for the period of 1988–2001 using the NCEP 3-day mean wind stress forcing.

c. Experiments

HYCOM is first forced by the 3-day mean fields described in section 2a for the period of 1988–2001 (see Table 1). This solution includes effects of intraseasonal atmospheric forcing and is referred to as the OGCM main run (OGCM_MR). To estimate the role played by oceanic instabilities in causing the 30–60-day oscillation, HYCOM is also forced by the monthly fields, which excludes the intraseasonal atmospheric forcing. This solution is referred to as the OGCM background run (OGCM_BR), and it is discussed in section 3d.

To understand the role played by wind driven, equatorial wave dynamics, the LM without the Maldives Islands is forced by the 3-day mean wind stress field. It is referred to as the linear model main run (LM_MR; see Table 1). To isolate effects due to direct wind forcing and reflected waves, a damper in the eastern equatorial ocean is applied (see McCreary et al. 1996 and Han et al. 1999 for detailed descriptions of the damper). The damper efficiently absorbs the energy of equatorial Kelvin waves so that almost no Rossby waves are reflected back into the ocean interior from the eastern ocean boundary. Thus, the damped solution is independent of reflected Rossby waves. It is referred to as the "directly forced" response and is denoted as the linear model forced run (LM_FR). (With this definition, the forced response includes effects due to Kelvin waves reflected from the western boundary. Nevertheless, it

still is a useful measure of the part of the solution that is directly forced by the wind.) Consequently, the *difference* between the LM_MR and LM_FR represents effects of Rossby waves reflected from the eastern boundary, referred to as the "reflected wave" response. To test the effect of the Maldives Islands on equatorial wave propagation, the Maldives are included in an additional run, which is otherwise identical to the LM_MR, and this solution is referred to as LMMD_MR. Additionally, a series of LM experiments forced by idealized winds are performed to demonstrate resonance, and these experiments are described in detail in section 3c(2)i.

3. Results

In section 3a, the OGCM_MR is compared with observations to verify the model performance. In section 3b, the OGCM and LM intraseasonal variabilities are described, and both the maximum spectral peak at 90 days and secondary peaks at 30–60-day periods are shown. In section 3c, a detailed discussion of the origin and dynamics of the 90-day oscillation is provided. Finally, in section 3d dynamics of the 30–60-day variations are discussed, and the relative importance of intraseasonal winds versus oceanic instabilities is estimated.

a. OGCM_MR and observations

The longest observed current record in the equatorial Indian Ocean during the model integration period is the WOCE current meter data at (0°N, 80.5°E), which lasted for approximately 13.5 months during 1993/94. Time series of WOCE and OGCM_MR intraseasonal zonal currents at 50, 281, and 578 m are shown in Fig. 3. For both the simulated and observed records, the intraseasonal currents shown in Fig. 3 are obtained by first removing the harmonics with periods longer than 90 days from the original records, and then performing a 15-day boxcar running average, in order to highlight variability on 30–60-day scales. Unless otherwise specified, all intraseasonal variabilities discussed in later sections are obtained in this manner. At both the surface and subsurface levels, the OGCM is able to capture much of the observed intraseasonal variations, with a model–data correlation coefficients of 0.53 at 50 m, 0.63 at 281 m, and 0.43 at 578 m, all of which are above 95% red noise significance. (Note that at 578 m, observed/modeled currents from mid-October to mid-November are shifted out of phase. When this portion of data is removed, the correlation is 0.64.) At seasonal time scales, the modeled and observed currents agree very well (Han et al. 2004).

To provide a quantitative comparison between the observed and modeled intraseasonal sea level, Fig. 4 shows the time series of intraseasonal SLA during 1995–98 in the central and eastern equatorial basin

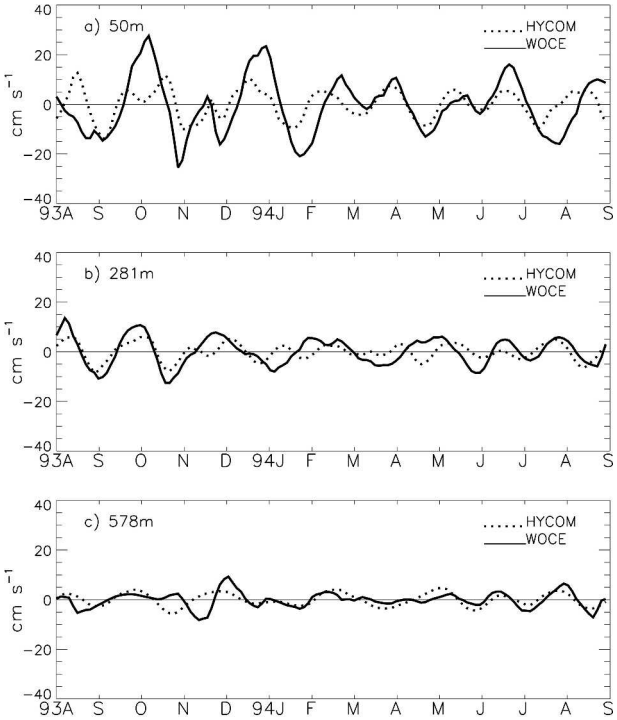

FIG. 3. (a) Intraseasonal components of zonal currents (cm s^{-1}) in the central equatorial Indian Ocean (0°N, 80.5°E) observed by WOCE current-meter data during Aug 1993–Aug 1994 at 50-m depth (solid curve), and intraseasonal currents from OGCM_MR at the same depth (dotted curve). (b) Same as (a) but for currents at 281-m depth. (c) Same as (a) but for currents at 578-m depth.

(Figs. 4a,b, respectively), where TOPEX sea level shows maximum 90-day spectral peaks with distinct spatial structures (Fig. 1; section 1a). Note that the 3-day mean OGCM SLA is interpolated to the TOPEX resolution of 10 days before the comparison. The observed intraseasonal sea level variations (solid lines) are reasonably simulated by OGCM_MR (dotted lines), although the modeled SLAs are underestimated in the central basin (Fig. 4a). The correlation coefficients between the observed and simulated curves are 0.54 in the central and 0.69 in the eastern basin. Both exceed 95% red noise significance level. Noticeable 90-day variations can be identified in the figure. Further comparisons between the modeled and observed sea level spatial structure are shown in Fig. 8 of section 3c(1).

The reasonable agreement between the simulated and observed surface and subsurface variabilities suggests that the OGCM has captured the major physics that determine the intraseasonal variabilities. There are, however, some notable differences. For example, the model–data currents at 578-m depth are opposite in phase during mid-October to mid-November of 1993 (Fig. 3c). These discrepancies may be due in part to uncertainties in the forcing fields (Han et al. 2004).

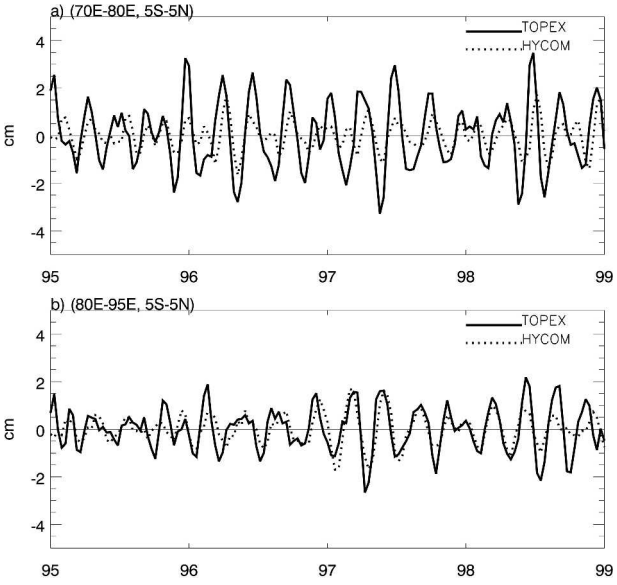

FIG. 4. (a) Time series of intraseasonal SLA (cm) during 1995–98 averaged over the central equatorial basin (5°S–5°N, 70°–80°E) from TOPEX/Poseidon altimeter data (solid curve) and from the OGCM_MR (dotted curve). (b) Same as (a) but for averaging over the eastern basin (5°S–5°N, 80°–95°E).

b. Intraseasonal variability

The time evolution of the intraseasonal component of the mixed layer zonal current u_m along the Indian Ocean equator from the OGCM_MR solution during 1993–97 is displayed in Fig. 5a. To better represent the surface current, here the depth of the mixed layer is defined to be the first depth at which the density increase relative to the surface density corresponds to a 0.2°C drop in temperature. For comparison, the intraseasonal zonal current averaged over the upper 20 m from solution LM_MR is shown in Fig. 5b. Zonal surface currents in the equatorial Indian Ocean exhibit strong intraseasonal fluctuations, with an amplitude of as much as 65 cm s^{-1} (Fig. 5a). These intraseasonal currents are well reproduced by the LM (Fig. 5b), suggesting that the wind-driven, equatorial wave dynamics play a crucial role in determining the observed intraseasonal oscillations in the equatorial Indian Ocean.

Given the importance of winds in causing the intraseasonal currents, Fig. 6a shows variance spectra of NCEP 3-day mean zonal wind stress, τ^x, based on a 12-yr record during 1990–2001. The corresponding variance spectra for zonal surface current, u_m, from solution OGCM_MR is shown in Fig. 6b. Consistent with the Han et al. (2001a) intermediate ocean model study, spectral maxima for τ^x occur at 30–60-day periods, whereas the maximum peak of u_m occurs at 90 days, dominating the u_m peaks at 30–60-day periods. The shift of dominant peak frequency between the forcing and response fields suggests that the equatorial Indian Ocean selectively responds to forcing by the 90-day winds.

The dominance of the 90-day peak over the 30–60-day ones appears not only at the oceanic surface, but also extends to greater depths (Figs. 6c, d). Variances for both the 90- and 30–60-day spectral peaks, however, decrease quickly with the increase of depth (note the scale change in each plot), suggesting that most energy is surface trapped, while a small portion propagates down to the deep ocean. Interestingly, the 90-day peak appears to move progressively westward with increasing depth: It occurs near 80°E at the surface (Fig. 6b), shifts to 63°E at 300 m, and to 53°–62°E at 600 m (Figs. 6c, d).

c. The near 90-day variation

Given the dominance of the 90-day spectral peak at the intraseasonal period, in this section a detailed investigation of its origins and dynamics in the surface and subsurface layers will be provided.

1) KELVIN AND ROSSBY WAVE STRUCTURE AT THE SURFACE

The strong 90-day peak of zonal currents from the OGCM_MR corresponds to the large 90-day peak in the TOPEX/Poseidon sea level observations (Fig. 1). This correspondence is further demonstrated in Fig. 7, which shows an equatorially trapped structure for intraseasonal zonal flow. Variance of the 90-day zonal surface currents reaches a maximum at the equator all across the basin, and decreases poleward in the eastern basin (Fig. 7c), which is a typical feature of equatorial Kelvin waves. In the central basin, there are weaker peaks on each side of the equator at the 90-day period (Figs. 7a, b), which is a typical structure of first meridional mode ($l = 1$) Rossby waves. These results, combined with the sea level patterns from the TOPEX/Poseidon satellite data (Fig. 1), suggest that these 90-day equatorial Kevin and Rossby waves are largely forced by the 90-day winds.

To further demonstrate this point, the 90-day SLA and surface current from solution OGCM_MR, the 90-day SLA from TOPEX/Poseidon satellite altimeter data, and the 90-day NCEP surface wind stress are extracted by harmonic analysis. The "90-day" variation is represented by the sum of harmonics with periods between 75 and 100 days. Figure 8 shows the simulated current and SLA (left), and the observed SLA and NCEP wind stress (right) during a 90-day oscillation that occurs at the beginning of 1997. During the easterly phase of the 90-day wind (arrows in Fig. 8d), sea level drops in the east with a maximum amplitude occurring near the equator and decreasing poleward (fill and line contours in Figs. 8a,d), which is a typical structure of equatorial Kelvin waves. At the same time, in the central basin two SLA maxima occur on either side of the equator, which is a typical structure for $l = 1$ Rossby waves. These SLA patterns appear in both the TOPEX data and the OGCM solution, indicating that the spatial

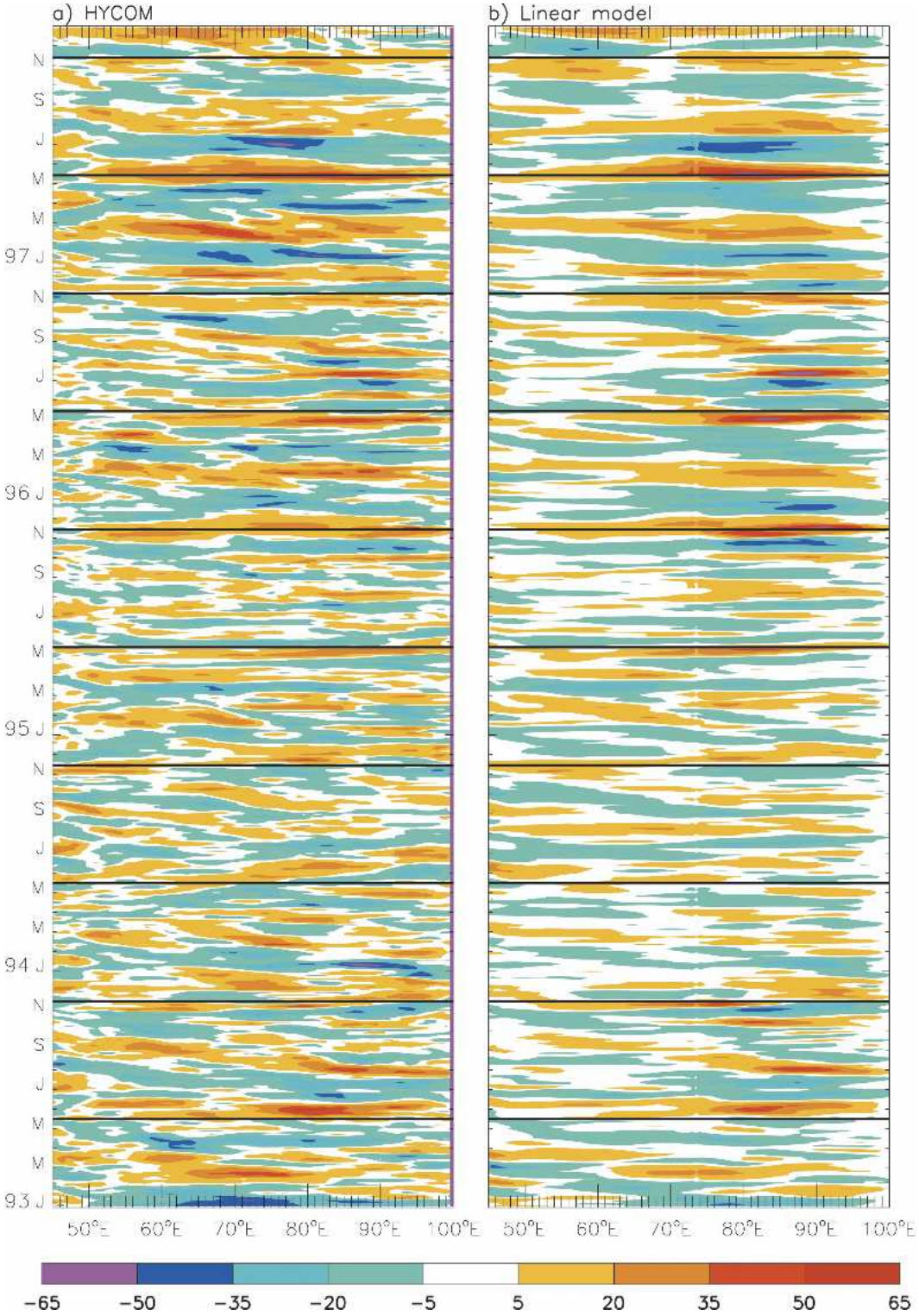

FIG. 5. (a) Longitude–time plot of intraseasonal component for zonal current (cm s^{-1}) in the surface mixed layer, u_m, along the Indian Ocean equator (averaged over 2°S–2°N) from solution OGCM_MR for the period of 1993–97, the solution that includes all intraseasonal forcing. (b) Same as (a) but for intraseasonal zonal currents averaged in the upper 20 m from LM_MR.

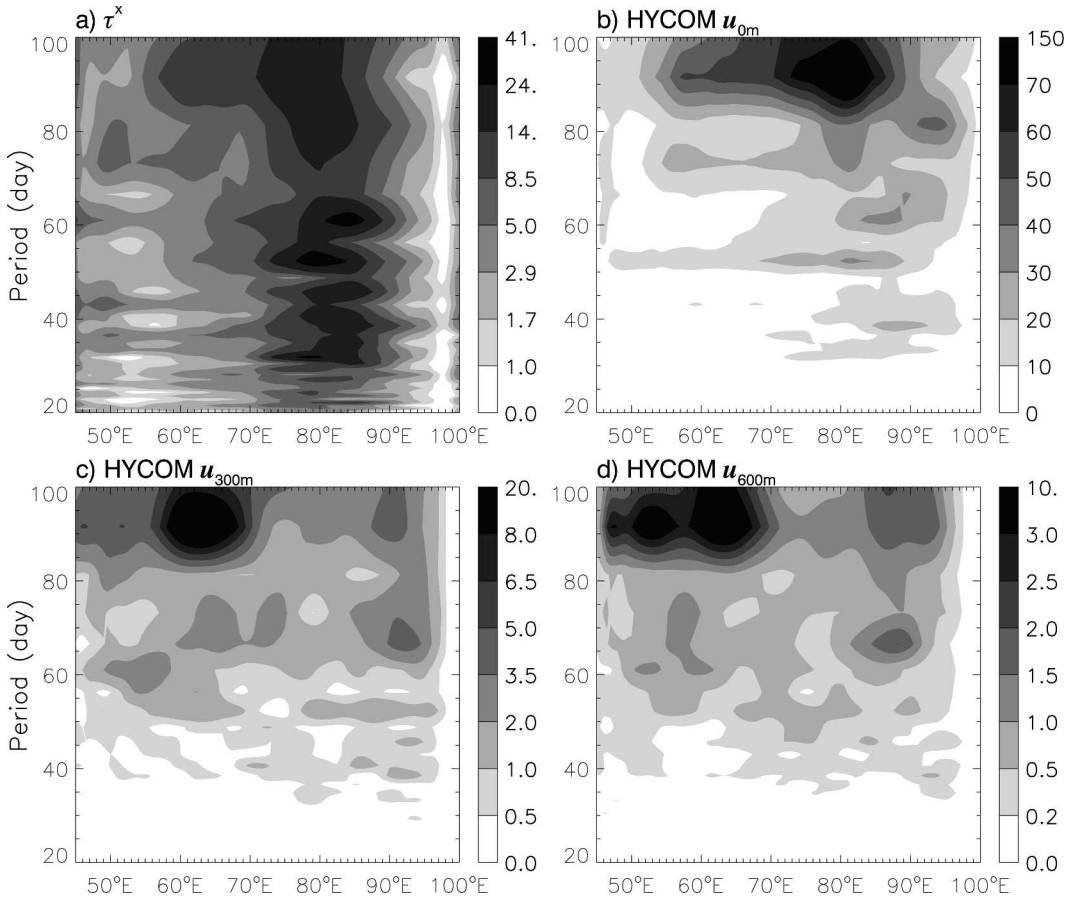

FIG. 6. (a) Variance spectra for 3-day mean NCEP–NCAR zonal wind stress along the Indian Ocean equator (averaged over 2°S–2°N), based on a 12-yr record (1990–2001). Variance at periods of 20–100 days is plotted. Units: 10^{-6} dyn^2 cm^{-4}. (b) Same as (a) but for variance spectra for 3-day mean zonal surface mixed-layer currents from OGCM_MR. Units: cm^2 s^{-2}. (c), (d) Same as (b) but for depths of 300 and 600 m, respectively.

structure of the 90-day SLA is well simulated by HYCOM. Associated with the SLAs are westward surface currents along the equator and anticyclonic gyres around the off-equatorial SLA maxima. Forty days later, currents and SLAs reverse with the reversal of the winds (Figs. 8b,e). Ninety days later, currents and SLAs reverse again (Figs. 8c,f), completing a 90-day cycle.

Figure 9 shows longitude–time plots of observed SLA at 5°S (left) and 5°N (right). The SLA maxima near both 5°S and 5°N propagate westward as Rossby waves, with a speed of $c_r = 55$ cm s^{-1} estimated by the dotted line that connects "A" and "B" in Fig. 9b. For the $l = 1$ Rossby wave, its speed $c_r = c/3$, the estimated baroclinic mode speed $c = 165$ cm s^{-1}, which is very close to the second baroclinic mode speed of the Indian Ocean (167 cm s^{-1}; section 2b).

2) DOMINANCE OF THE 90-DAY VARIATION

The dominance of the 90-day spectral peak over the 30–60-day one appears in solution LM_MR at both the surface and subsurface levels (left panels of Fig. 10), which confirms the importance of wind-driven equatorial wave dynamics in causing the 90-day oscillation. Note that the 90-day variance maxima shift westward with depth, as they do in the OGCM solution (Fig. 6).

There are, however, quantitative differences between the OGCM and LM solutions. They are largely due to the presence of the background mean flow in the OGCM, which may alter the propagating speeds of Kelvin and Rossby waves, affect their vertical structure, and absorb their energy at critical layers (McPhaden et al. 1987). These effects act the least on the low-order baroclinic waves, because higher-order mode Kelvin and Rossby waves can rarely reach the deep ocean due to friction and critical layer absorption. Hence, it is the low-order baroclinic mode waves that carry energy into the deep ocean in both the OGCM and linear solutions (Rothstein et al. 1985; McPhaden et al. 1986). Despite their differences, the OGCM and linear solution bear a remarkable resemblance to each other at intraseasonal time scale, and this similarity builds the foundation for

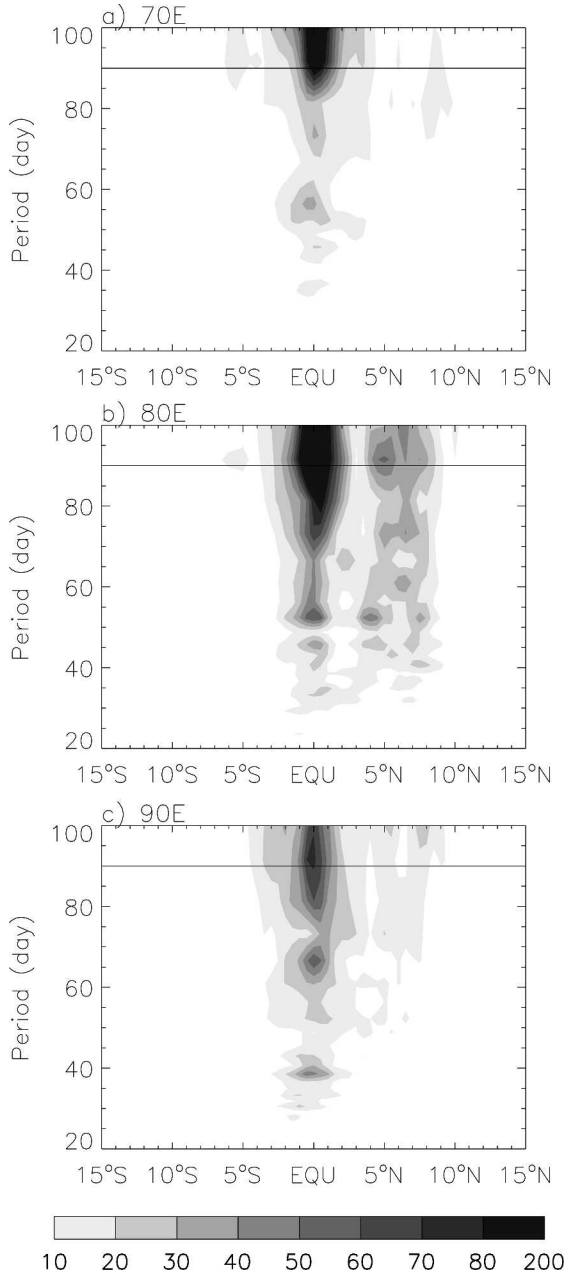

FIG. 7. (a) Meridional section at 70°E for the variance spectra of 3-day mean zonal surface currents ($cm^2\ s^{-2}$) from solution OGCM_MR, based on the solutions for the period of 1990–2001. (b), (c) Same as (a) but for meridional section at 80° and 90°E, respectively.

using the LM to understand the dynamics of the 90-day variation.

(i) Directly forced response and reflected waves

Interestingly, the 90-day spectral peaks are considerably weakened in both the surface and subsurface layers in solution LM_FR, the solution after the Rossby waves reflected from the eastern ocean boundary are removed from the total solution LM_MR (right panels of Fig. 10). The large contrast between solution LM_MR and solution LM_FR reveals that Rossby waves reflected from the eastern ocean boundary tend to intensify the directly forced response in the ocean interior.

To further understand this selective response, a series of 26 LM experiments are performed in which the LM is forced by a series of idealized winds with periods $T = 30, 33, 36, \ldots, 105$ days. For each experiment, the LM is forced by a zonal wind stress with an amplitude of 0.25 dyn cm^{-2} and with a spatial structure centered at 80°E on the equator, decreasing to zero as a cosine function at 50°E, 100°E, 5°N, and 5°S, similar to the equatorial portion of the 90-day winds. The only difference among the experiments is the difference in forcing frequency.

Figure 11a shows surface current maxima at each forcing period T from the 26 experiments for the sum of the first 25 baroclinic modes (solid curve). Similar experiments are performed for the directly forced response (dotted curve), in which the damper is applied in the LM. The difference between the two curves measures the reflected wave contribution. The response (solid curve) reaches a maximum amplitude near the 90-day period, indicating that the equatorial Indian Ocean selectively responds to the 90-day wind. This selective response results largely from the reflected waves, because the directly forced response does not produce a distinct 90-day peak (dotted curve). The directly forced response, however, does increase with the forcing period, and so contributes to larger current amplitudes at the lower frequency side of the intraseasonal band.

The selective response of reflected waves at the 90-day period results almost entirely from the first two baroclinic modes (Fig. 11b). Mode 2 explains a large portion but mode 1 also contributes (Fig. 11c). Interestingly, the directly forced response of the first two baroclinic modes (dotted curve of Fig. 11b) increases with the increase of period from 30 to 85 days and thereafter remains almost constant. For the higher order modes, the solid and dotted curves almost coincide (Fig. 11d), indicating that there is no significant enhancement from the reflected waves.

(ii) Resonance

When the forcing is periodic, reflected waves can act to enhance the directly forced response. When the forcing period T satisfies

$$T = \frac{4L}{mc_n}, \tag{1}$$

resonance occurs (Cane and Sarachik 1981; Cane and Moore 1981). In this case, reflected waves intensify the

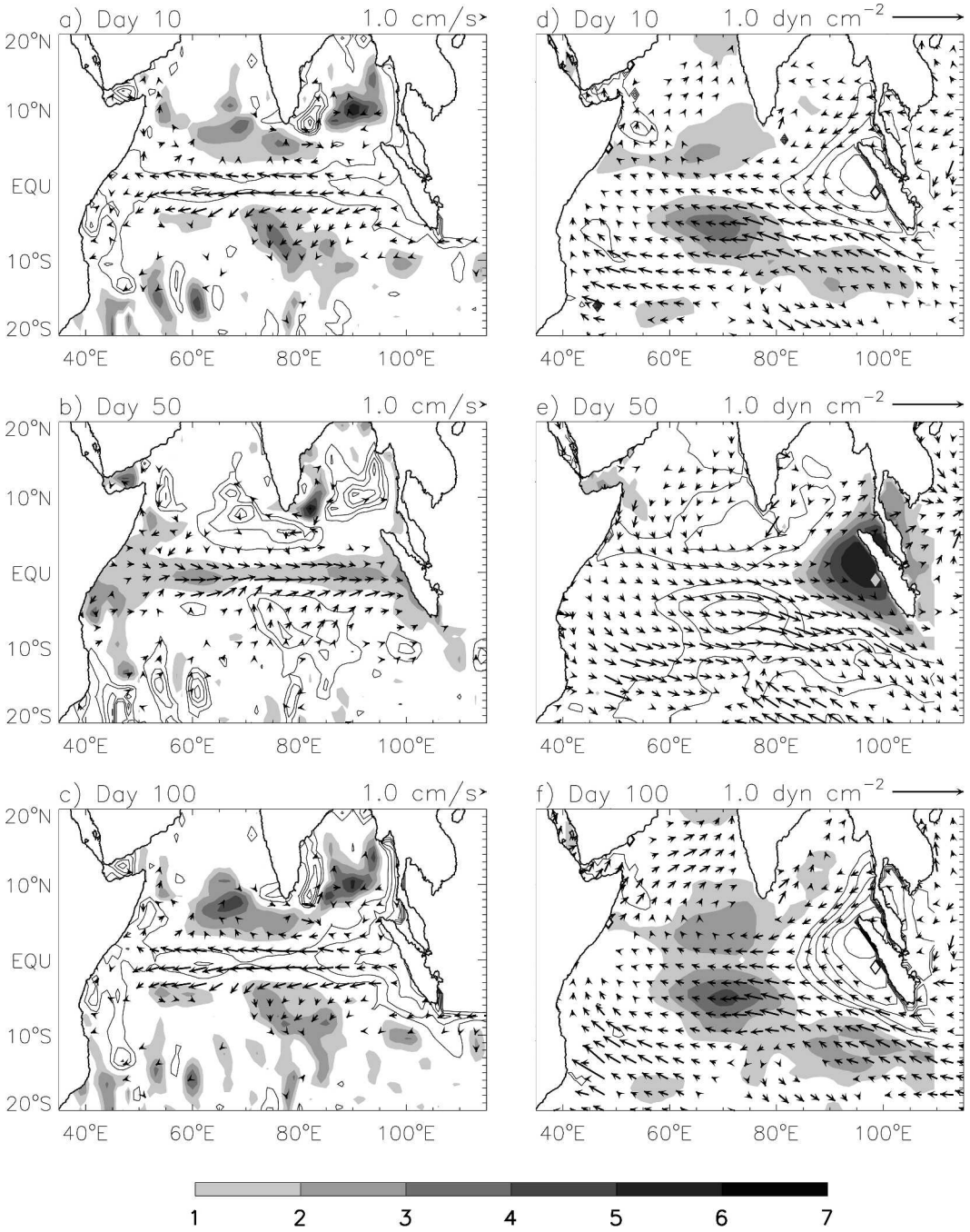

FIG. 8. The 90-day SLA (cm; fill and line contours) and 90-day surface currents (cm s^{-1}; arrows) for (a) day 10, (b) day 50, and (c) day 100 of 1997. The 90-day NCEP wind stress (dyn cm^{-2}; arrows) and 90-day TOPEX/Poseidon altimeter data (fill and line contours) for (d) day 10, (e) day 50, and (f) day 100 of 1997. Positive values for SLA are shaded and negative ones are contoured, with an interval of 1 cm. Zero contours are suppressed.

directly forced response. In the above equation, L is the basin width of the equatorial Indian Ocean, and m is a positive integer. For the size of the equatorial Indian Ocean basin, $L = 6327$ km. For $T = 90$ days, it yields resonance mode speed of $c_n = 325$ cm s^{-1} when $m = 1$ and $c_n = 163$ cm s^{-1} when $m = 2$. Thus, the resonance mode speed for $m = 2$ is very close to the Indian Ocean second baroclinic mode speed of $c_2 = 167$ cm s^{-1}, suggesting that the second baroclinic mode resonates with the 90-day wind in the equatorial Indian Ocean. The first baroclinic mode speed of the Indian Ocean is $c_1 = 274$ cm s^{-1}, which is about 50 cm s^{-1} slower than the

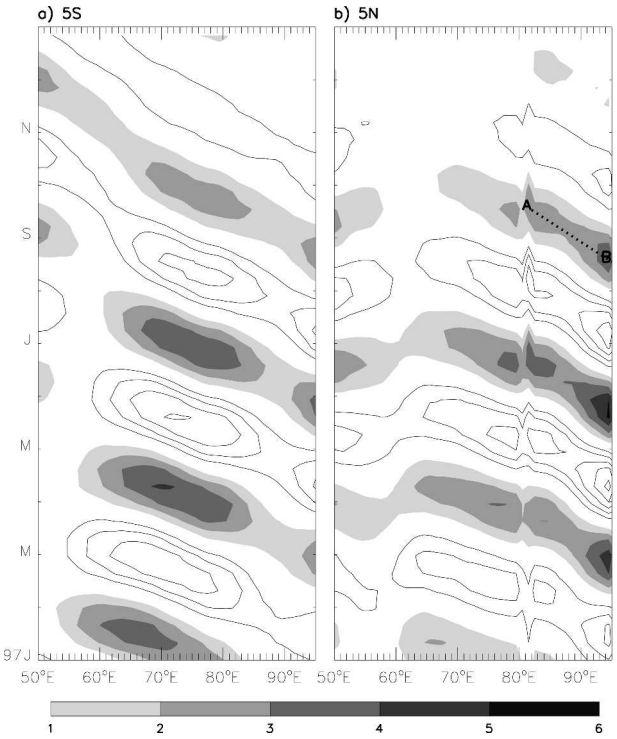

FIG. 9. Longitude–time plot of 90-day SLA (cm) from TOPEX/Poseidon satellite altimetry data during 1997 at (a) 5°S and (b) 5°N.

resonance mode speed when $m = 1$, but it is still close enough to show some contribution.

As demonstrated by Cane and Moore (1981), the sum of a Kelvin wave and its eastern boundary reflection obtains the maxima at

$$x = x_e - \frac{\pi c_n}{4\omega}(2m + 1), \tag{2}$$

where x_e is the location of the eastern boundary, ω is the wave frequency, and $m = 0, 1, 2, \ldots$ is a positive integer. For $T = 90$ days and $x_e = 97°$E, the sum of Kelvin and reflected Rossby waves attains a maximum near 82°E for $m = 0$, a location that is very close to the maximum of the directly forced response (Fig. 10). For the first baroclinic mode, the maximum amplitude occurs at 73°E, which also intersects the peak of the directly forced currents. The resonant response of the second baroclinic mode, and to a lesser degree, the first mode, explains the large amplitude response in the ocean interior.

(iii) Preferential excitation of low-order mode Kelvin and Rossby waves

For the first and second baroclinic modes, Rossby waves exist for periods longer than 32 and 40 days, respectively (Fig. 12). Their response is nearly inviscid because effects of friction are inversely proportional to c_n^2 (McCreary 1980). Assume the ocean is forced by a zonal wind stress τ^x, the amplitudes of Kelvin or Rossby waves are proportional to the zonal integral of the product of the wind and wave structure, $\int \tau^x e^{-ikx}\, dx$, where k is the wavenumber of Kelvin or Rossby waves. The amplitude thus depends on the parameter kL, where in this case L represents the zonal scale of the wind. If $kL \geq 1$, then e^{-ikx} oscillates within the region of the wind, producing an oscillating integral; when $kL \ll 1$, $e^{-ikx} = 1$ and the amplitude achieves the maximum possible value. At lower frequencies, both Kelvin and Rossby waves have longer wavelengths and thus lower wavenumbers (Fig. 12). They are therefore more efficiently excited by the large-scale winds than higher-frequency waves, which have shorter wavelengths and higher wavenumbers (Fig. 11b). In another words, there is a coupling between the wind and wave structures, in that the lower-frequency Kelvin and Rossby waves couple better with the large-scale winds, and thus they are more efficiently excited by such winds.

(iv) Response of intermediate and high-order modes

For baroclinic modes with $n \geq 3$, the total solution results almost entirely from the directly forced response, and current amplitudes increase with the increase of period (Fig. 11d). The slight difference between the total solution and the directly forced response occurs primarily at lower frequencies, and this difference is caused by the intermediate modes ($3 \leq n \leq 8$; Fig. 11e). For the high-order modes ($9 \leq n \leq 25$), the two curves are identical (Fig. 11f).

High-order mode Rossby waves are not available for $T \leq 90$ days (Fig. 12). Thus, the high-order response results entirely from the directly forced Kelvin wave, which explains why the total and directly forced curves are identical in Fig. 11f. In addition, because friction acts strongly on these modes due to their slower speed c_n, the high-order response is "local" to the forcing winds, that is, the zonal pressure gradient is dominated by friction in the zonal momentum equation (McCreary 1980). For a periodic zonal wind stress forcing $F_n e^{-i\omega t}$ where $\omega = 2\pi/T$, zonal momentum equation for a high-order mode n at the equator can be approximated by

$$u_{nt} + \frac{A}{c_n^2} u_n = F_n e^{-i\omega t}, \tag{3}$$

where $A = 0.000\,13\ \text{cm}^2\ \text{s}^{-3}$ for the LM as in Moore and McCreary (1990).

The solution to Eq. (3) is $u_n = F_n e^{-i\omega t}(-i\omega + A/c_n^2)^{-1}$, and thus amplitude $|u_n|$ satisfies

$$|u_n|^2 = \frac{F_n^2}{\omega^2 + \dfrac{A^2}{c_n^4}}. \tag{4}$$

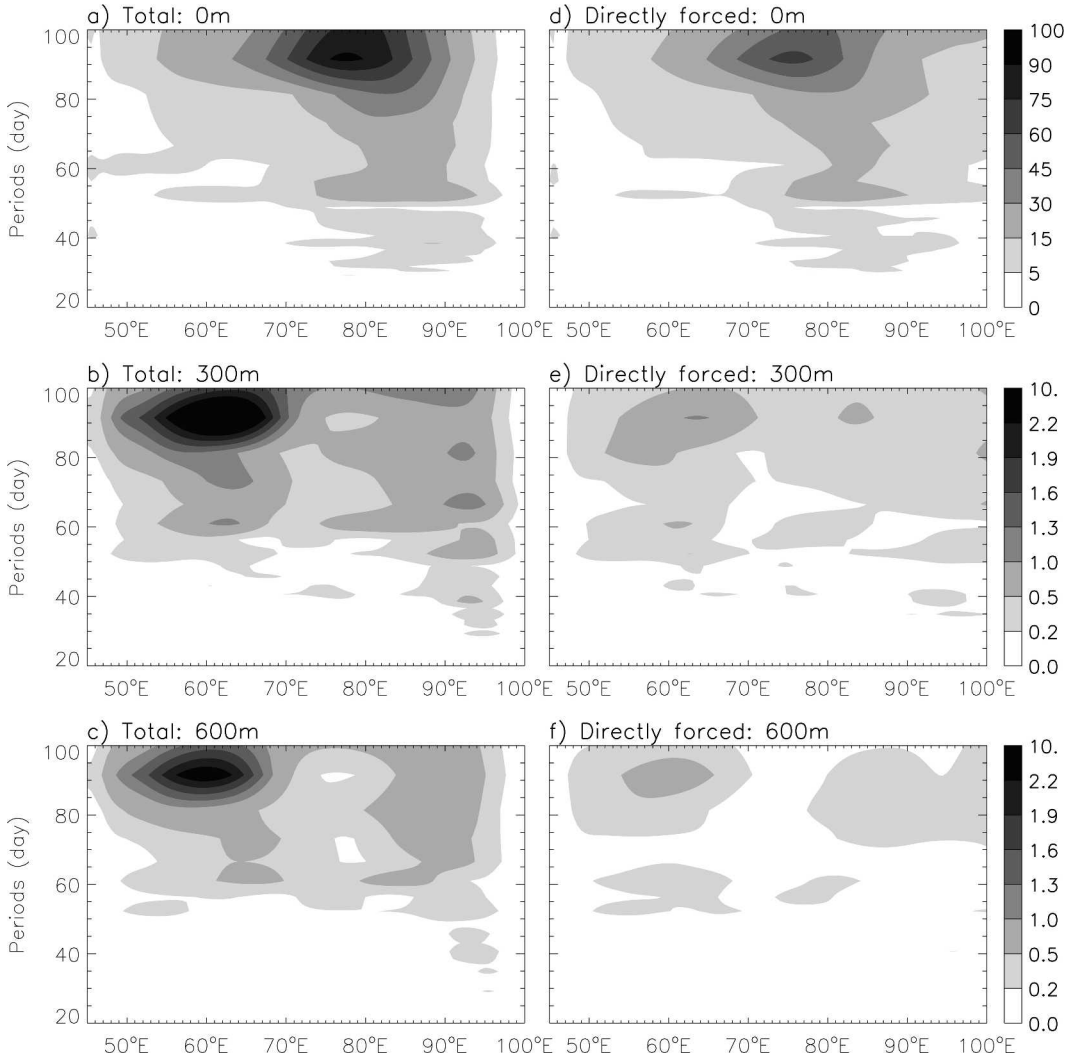

FIG. 10. Variance spectra ($cm^2\ s^{-2}$) along the Indian Ocean equator (averaged over 1°S–1°N) for 3-day mean zonal currents from LM_MR at (a) the surface and depths of (b) 300 and (c) 600 m, based on the solutions for the period of 1990–2001. (d)–(f) Same as (a)–(c) but for solution LM_FR, which estimates directly forced response that is independent of Rossby waves reflected from the eastern ocean boundary.

For period $T < 90$ days, $A^2/c_n^4 \ll \omega^2$ holds for the high-order modes with $9 \leq n \leq 25$. For example, for mode 10 whose $c_{10} = 30\ cm\ s^{-1}$, $A^2/c_{10}^4 = 2 \times 10^{-14}$; $\omega^2 = 146 \times 10^{-14}$ for $T = 60$ days and $\omega^2 = 83 \times 10^{-14}$ for $T = 80$ days. As long as $A^2/c_n^4 \ll \omega^2$, $|u_n|$ will increase with T. Consequently, responses of the high-order modes are local to the winds, since $u_n = 0$ outside the wind forcing region where $F_n = 0$. Within the wind-forcing region, amplitudes of currents are proportional to F_nT. For a given period T, amplitude of u_n is proportional to wind strength F_n. Stronger winds drive stronger currents. For a given wind strength F_n, response of current is proportional to the forcing period T. A longer period of forcing causes a stronger current. Solution (4) explains why the current amplitudes of the high-order modes increase monotonically with the increase of period in Fig. 11f.

For the intermediate modes, Rossby waves do not exist for periods shorter than 55 days (Fig. 12). Consequently, the intermediate mode response is directly forced at $T < 55$ days, and this explains the coincidence of the total and directly forced curves at shorter periods (Fig. 11e). At lower frequencies, Rossby waves become available. For example, at 90-day period, Rossby waves are available for all the intermediate modes. Reflected waves associated with these modes tend to cancel their directly forced response for periods of 90–105 days. In comparison with modes 1 and 2, the intermediate modes feel more friction due to the decrease of c_n. The increase of current amplitude with the increase of pe-

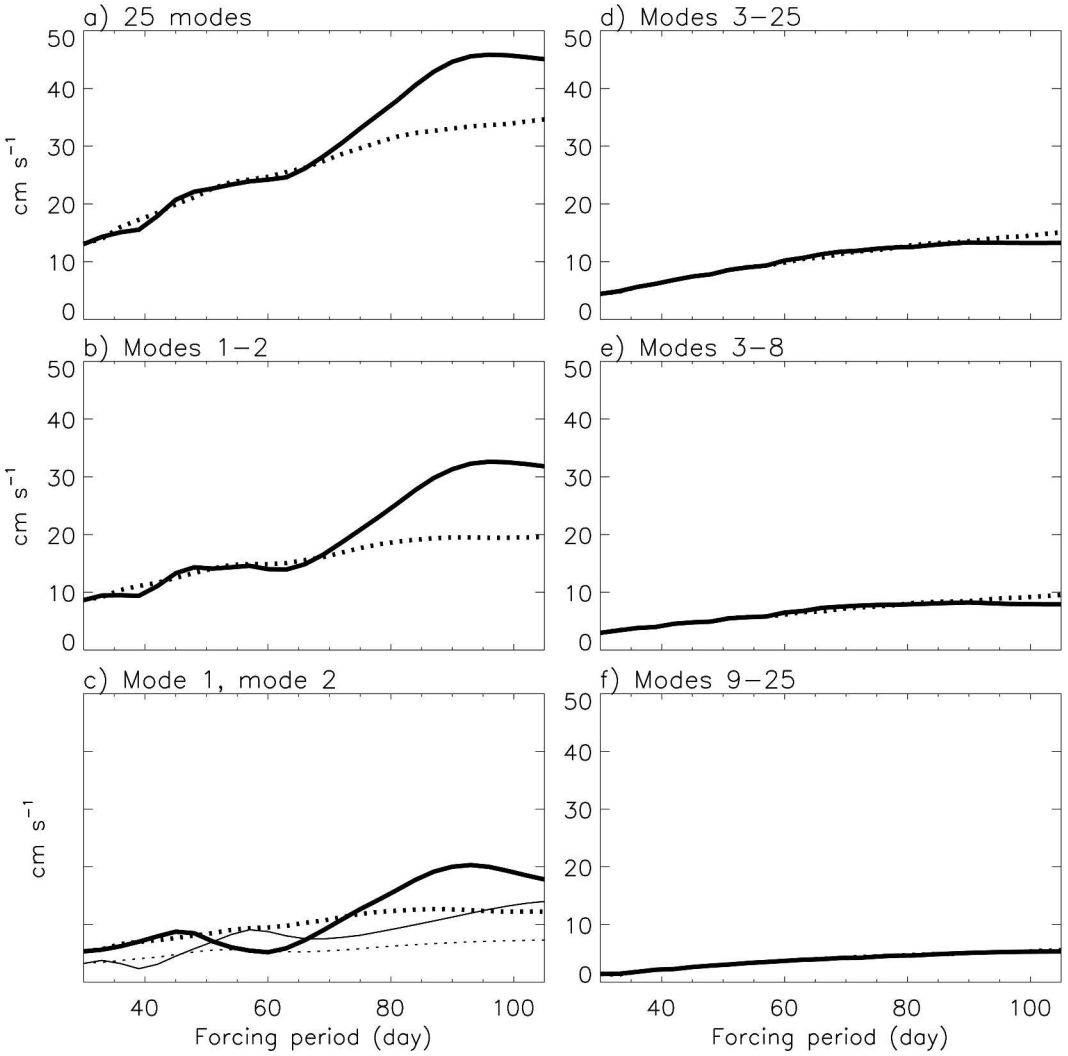

FIG. 11. Amplitudes of zonal surface currents (cm s^{-1}) from a series of experiments forced by a series of idealized zonal wind stress (see text for detail). The winds have the same amplitudes and spatial structure for each experiment and differ only in frequency, which varies from 30 to 105 days for every 3-day interval. (a) Sum of the first 25 baroclinic modes for the total solution (solid curve) and for the directly forced response (dotted curve). (b)–(f) Same as (a) but for (b) sum of the first two baroclinic modes, (c) mode 2 (thick curves) and mode 1 (thin curves), (d) sum of modes 3–25, (e) sum of modes 3–8, and (f) sum of modes 9–25.

riod for these modes results primarily from the preferential excitation of Kelvin and available Rossby waves at lower frequencies, analogous to the directly forced response of low-order modes.

3) VERTICAL PENETRATION

As shown in Fig. 6, most energy associated with the 90-day variation is trapped in the near surface layers above the thermocline. This surface trapping results from several processes: friction, pycnocline reflection, and critical layer absorption of Kelvin waves (Philander 1978; Philander and Pacanowski 1980, 1981; Gent and Luyten 1985; Rothstein et al. 1985; McPhaden et al. 1986, 1987). Rothstein et al. (1985) demonstrated that friction is the most important factor for surface trapping. Mixing acts strongly on the higher order modes, such that only low-order modes penetrate through the pycnocline into the deep ocean (Rothstein et al. 1985). As we shall see, in both the OGCM and LM solutions there is a fair amount of energy that penetrates through the pycnocline to the deep ocean (Figs. 6 and 10), and it is associated mainly with the first two baroclinic modes [cf. Fig. 10 (left panels) and Fig. 13], consistent with the conclusion of Rothstein et al. (1985).

In both the OGCM and LM solutions, the 90-day current maxima shift westward with depth (Figs. 6 and 10). This migration is also present in the directly forced response, although current amplitudes are significantly weakened without the reflected waves (right panels of

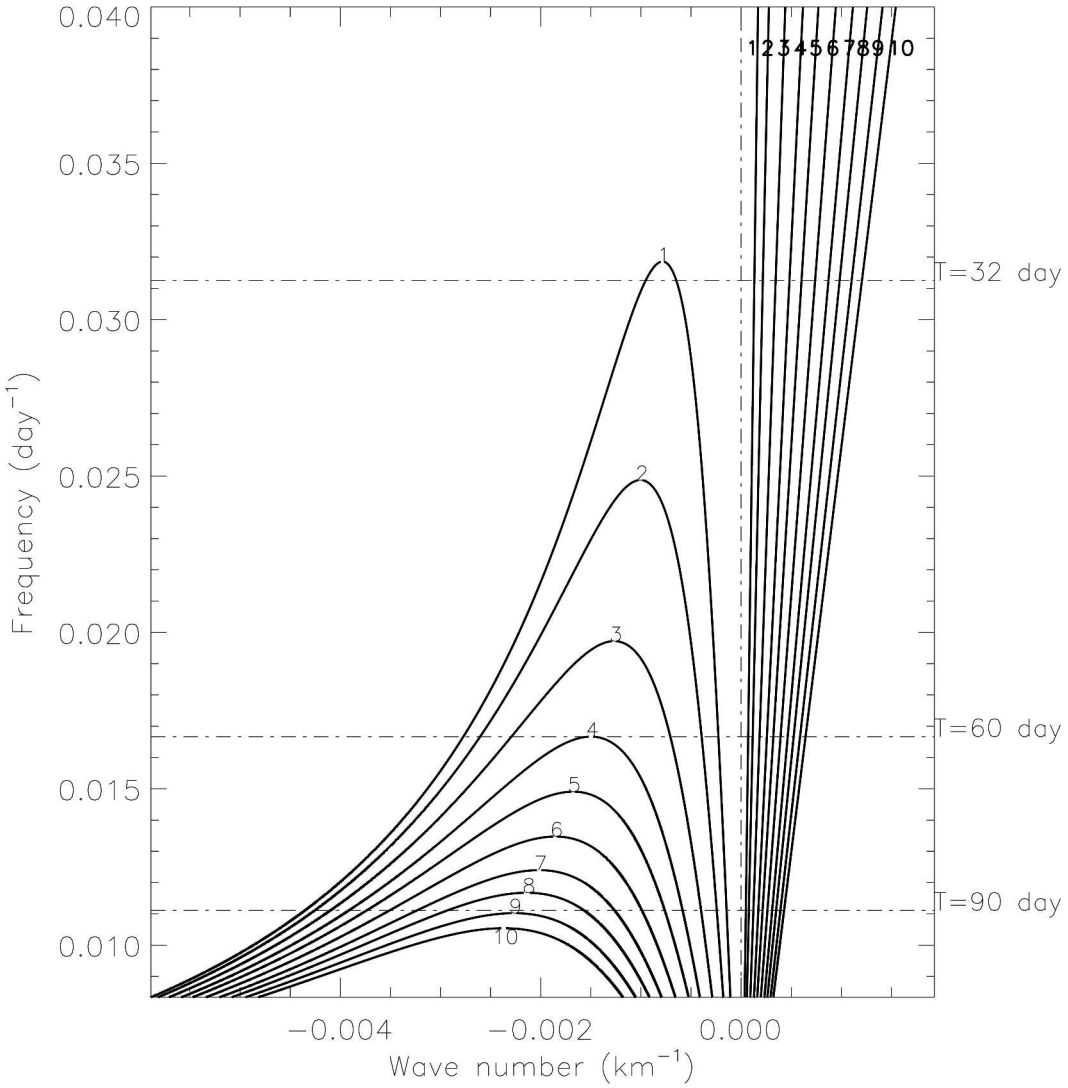

FIG. 12. Dispersion curves of Kelvin and $l = 1$ Rossby waves for the first 10 baroclinic modes ($n = 1, 2, \ldots, 10$).

Fig. 10). To understand this shift, Fig. 14 plots vertical sections of 90-day zonal currents from the idealized solution. As can be seen in Fig. 14a, the maximum amplitude shifts westward from 82°E at the surface to near 63°E at 600 m, similar to the 90-day spectral peaks in solutions OGCM_MR and LM_MR. This vertical structure is contributed from both the directly forced and reflected wave responses (Figs. 14c,e), and currents below 300 m are primarily associated with the first two baroclinic modes (cf. Figs. 14a,b).

This solution further confirms that only the low-order modes can penetrate through the pycnocline. For the directly forced response of the first two baroclinic modes (Fig. 14d), energy propagates down to the deep ocean along the WKB ray path (dashed curve in Fig. 14d) as a wide beam, which explains the westward shifting of the maximum 90-day variance in the directly forced solution (Figs. 10d–f). Energy associated with Rossby waves penetrates downward and westward into the deep ocean at an angle θ with the surface, where

$$\tan\theta = \frac{\omega}{N_b}(2l + 1), \tag{5}$$

and l is the meridional mode number of the Rossby waves. The ray path in Fig. 14d is calculated from the observed N_b used in the LM (see section 2b) with the choices of $T = 90$ days ($\omega = 2\pi/T$) and $l = 1$.

Reflected Rossby waves associated with the first two modes are almost equally important as the directly forced response in causing the westward shift of current maxima (Fig. 14f), because of constructive interference of the first and second baroclinic mode reflected waves near the surface and subsurface current maxima of the

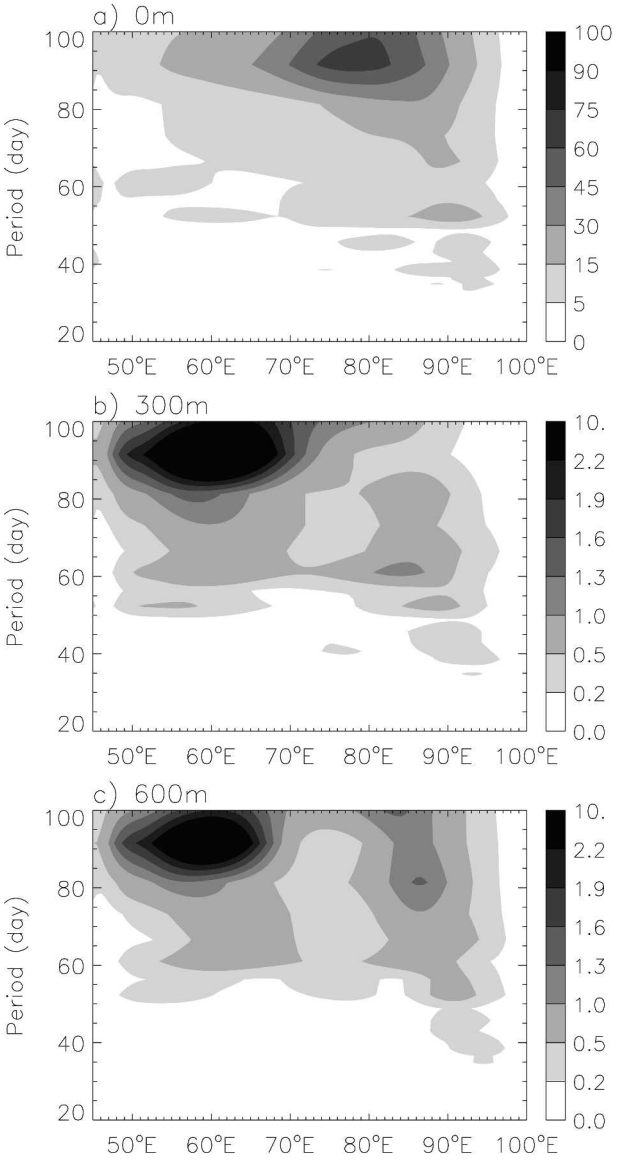

FIG. 13. Same as the left-side panels of Fig. 10 but for the response from the first two baroclinic modes.

total solution (Figs. 14g,h,a). As discussed in section 3c(2)ii, the maximum current of the second baroclinic mode is near 82°E, where Rossby waves reflected from the eastern boundary enhance the directly forced Kelvin wave (Figs. 14d,h). Because the $l = 1$ Rossby wave associated with the second baroclinic mode at $T =$ 90 days has a wavelength of 37° (Fig. 12), the reflected wave of the $n = 2$ mode reaches a minimum (negative) surface current near 63.5°E (Fig. 14h). Because the second baroclinic mode has a zero crossing near 170 m, current at the subsurface is positive (eastward) near 60°E, which enhances the directly forced Rossby waves ray at depth. Reflected waves associated with the first baroclinic mode interfere constructively with those of the second baroclinic mode near both the surface current maximum (near 82°E) and the subsurface current maximum (near 60°E; Fig. 14g).

4) EFFECTS OF THE MALDIVES ISLANDS

Because the Maldives Islands are located near the equator, they can affect the transmission of the equatorial waves and thus influence the resonance. Effects of the Maldives Islands on the seasonal cycle of equatorial surface currents have been examined in detail by Han et al. (1999). They suggested that the islands have little effect on the transmission of Kelvin waves, consistent with the conclusions of Yoon (1981) and Cane and du Penhoat (1982). In contrast, Rossby waves are affected much more, with some energy being reflected and some transmitted. To estimate this effect on the 90-day oscillation, the Maldives Islands are added in the linear model (section 2b). This solution is referred to as LMMD_MR. It is the same as LM_MR except for adding the Maldives.

Figure 15 shows the variance spectra of zonal currents along the Indian Ocean equator at 0, 300, and 600 m from solution LMMD_MR. East of the Islands the variances at both the surface and subsurface appear to be strengthened, whereas west of the Islands the variance especially the variance maxima at 300- and 600-m depths are weakened in comparison to solution LM_MR. These results may indicate that the Maldives weaken the westward transmission of Rossby waves and thus confine more energy in the eastern half of the basin, which is consistent with Han et al. (1999). Although somewhat weakened especially at the subsurface, the 90-day spectral peak still exists at all levels with the variance maxima shifting westward with depth, as in solution LM_MR. Therefore, the Maldives act to weaken the resonance somewhat but they do not alter the solution character.

5) POTENTIAL AIR–SEA INTERACTION

Consistent with the 90-day currents and sea level, observed Reynolds (Reynolds and Smith 1994) weekly sea surface temperature (SST) between 1982 and 2002 also shows a dominant 90-day peak over the intraseasonal period across the equatorial Indian Ocean (Fig. 16). The above discussion demonstrates that the equatorial Indian Ocean selectively responds to the 90-day wind forcing. This selective response may be the cause of the 90-day SST peak. Variation of the east-west SST gradient at the 90-day period, which is indicated by the zonal gradient of SST variance, may in turn act to enhance the 90-day winds, which may explain the westward extension of the 90-day zonal winds in the western basin (Fig. 6a). The enhanced zonal winds may feedback to the ocean, which further amplifies the 90-day response. A detailed understanding of the processes

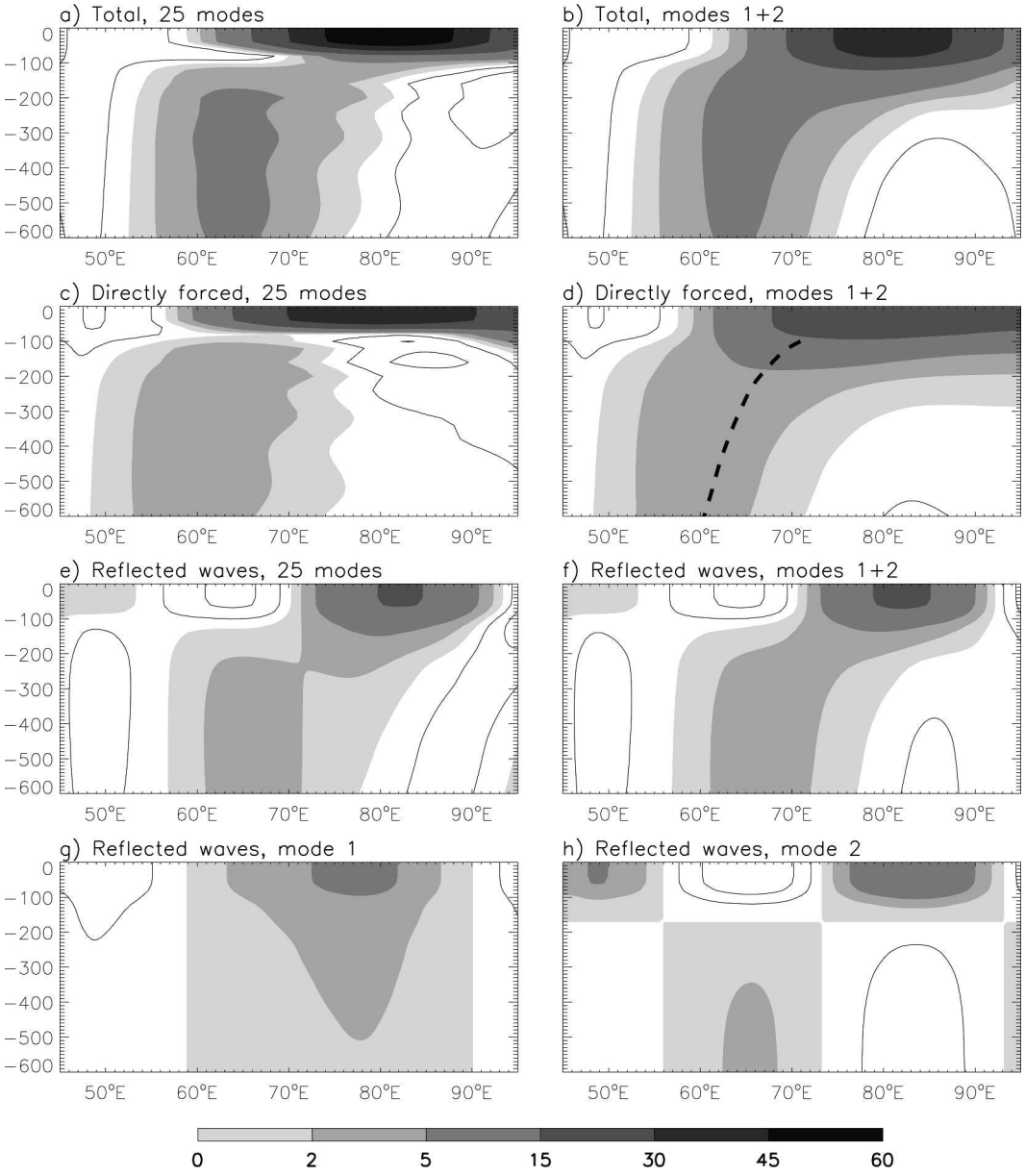

FIG. 14. Vertical sections of zonal current u (cm s^{-1}) above 600 m along the Indian Ocean equator (1°S–1°N average) from the idealized solution at the 90-day period (Fig. 11). (a) Total solution, 25 modes; (b) total solution, first two modes; (c) directly forced response, 25 modes; (d) directly forced response, first two modes: the dashed curve shows the WKB ray path for $l = 1$ Rossby waves at the 90-day period; (e) reflected waves, 25 modes; (f) reflected waves, first two modes; (g) reflected waves, mode 1; and (h) reflected waves, mode 2.

that determine the 90-day SST and its feedback to the atmosphere are out of the scope of this paper, but is an essential part of the ongoing research.

d. The 30–60-day variation

The 30–60-day currents have been observed at various locations of the equatorial Indian Ocean (section 1a), and are present in Figs. 6b–d as secondary spectral peaks. Although secondary in variance, the 30–60-day oscillation is much more frequently observed than the 90-day currents by direct current measurements. One reason for their frequent detection may be their relatively short period, which is more easily captured by the short data records. Unlike the 90-day current, which has a single peak, the 30–60-day current is composed of several relative peaks, and any peak that falls into 30–60-day period is referred to as the 30–60-day current. This feature also helps to increase the opportunity for their detection.

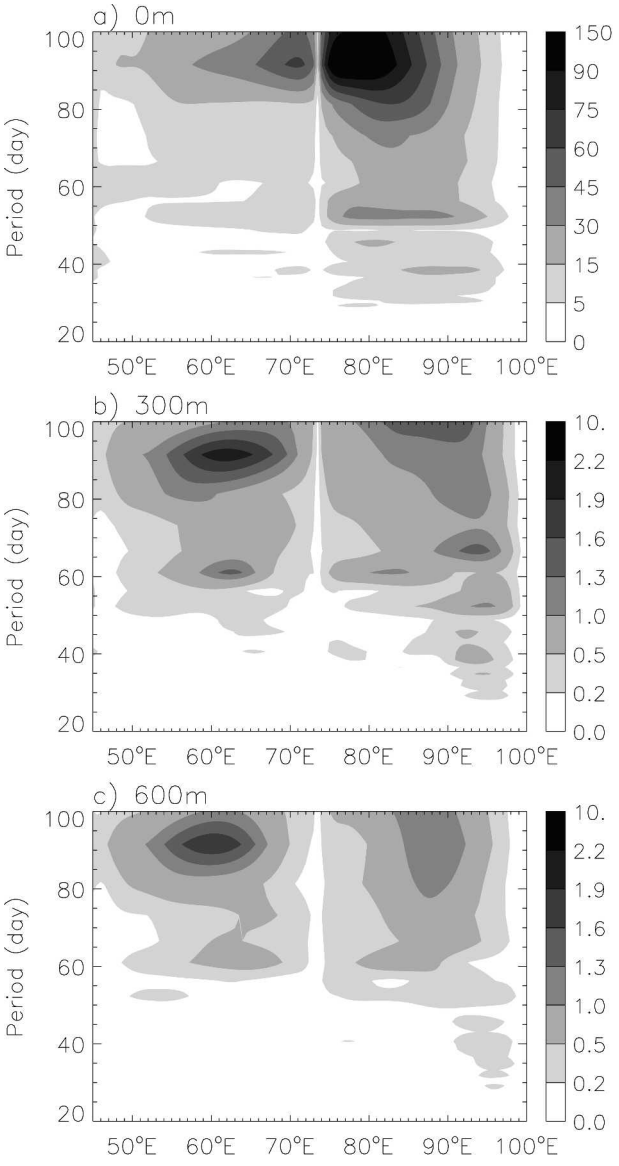

FIG. 15. Same as the left-side panels of Fig. 10 but for solution LMMD_MR, which includes the Maldives Islands. The Maldives are included as rectangular boxes along 73°–74°E at 0°–1°N and 2°–6°N.

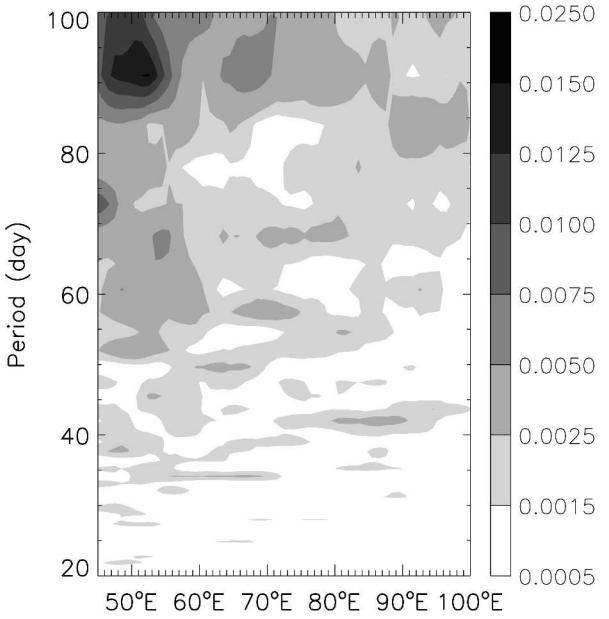

FIG. 16. Variance spectra (°C^2) of Reynolds weekly SST along the Indian Ocean equator based on the period of 1982–2002.

1) WIND-DRIVEN 30–60-DAY VARIATION

As for the 90-day variation, the 30–60-day currents are equatorially trapped (Fig. 7), and their energy can penetrate down to a few hundred meters in depth (Figs. 6 and 10). The 30–60-day spectral peaks occur in both the OGCM_MR and LM_MR, suggesting the deterministic role played by the intraseasonal winds in generating these currents. Near the surface, variance of the 30–60-day current remains essentially the same with and without the reflected waves (top panels of Fig. 10), indicating that currents at 30–60-day periods result primarily from the local response of high-order modes whose Rossby waves are evanescent, and from the directly forced Rossby and Kelvin waves which are available only for the low-order modes (Fig. 12). Amplitudes of currents associated with the low-order mode reflected waves are negligible compared to the directly forced response near the surface (top panel of Fig. 10). The spectral peaks of surface currents at 30–60-day periods, therefore, are directly forced by the strong peaks of winds at 30–60 days (Figs. 6 and 10).

In the deeper layers, the 30–60-day currents result primarily from the response of the first two baroclinic modes (Figs. 10 and 13), and reflected Rossby waves associated with the first two modes have a significant contribution relative to their directly forced part in the eastern basin (middle and lower panels of Fig. 10). In fact, current variance near 80°–90°E in the total solution results mostly from reflected Rossby waves, because energy rays associated with directly forced Kelvin waves penetrate down into the deep ocean with tan $\theta = \omega/N_b$, which is only ⅓ of that for the $l = 1$ Rossby wave. As a result, directly forced Kelvin waves have significant energy only near the surface in the eastern basin.

2) OCEANIC INSTABILITIES

Previous studies have pointed out the importance of oceanic instabilities in accounting for the near 50-day oscillation of zonal currents near the western boundary and in the central basin south of Sri Lanka (Kindle and Thompson 1989; Woodbury et al. 1989; Sengupta et al. 2001). Consistent with these studies, the OGCM

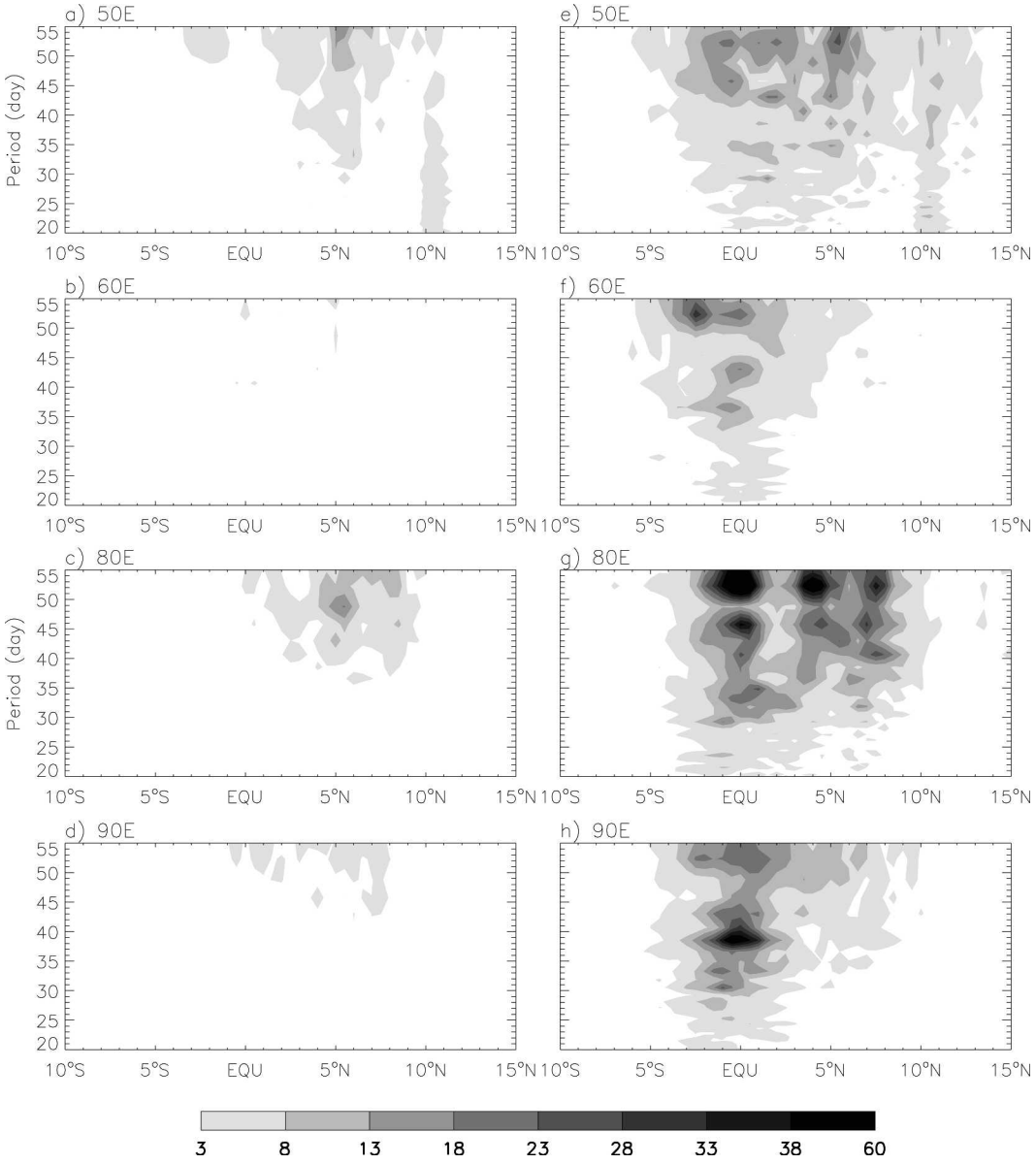

FIG. 17. Variance spectra ($cm^2\ s^{-2}$) of zonal surface currents u_0 along (a) 50°, (b) 60°, (c) 80°, and (d) 90°E from the OGCM_BR, the solution forced by monthly forcing fields. (e)–(h) Same as (a)–(d) but for OGCM_MR, the solutions forced by the 3-day mean forcing fields.

solution forced by monthly mean fields (OGCM_BR; Table 1) shows significant variance at 30–55-day periods near the western boundary and in the central basin south of Sri Lanka near 5°N (left panels of Fig. 17). These variances disappear in an LM solution forced by the monthly mean winds (not shown). These results suggest that oceanic instabilities do play a significant role in generating 30–60-day variations in the western basin and south of Sri Lanka. Forcing by intraseasonal winds, however, play a more important role overall (right panels of Fig. 17). Forcing by intraseasonal winds determines most of the amplitude of intraseasonal currents across the equatorial Indian Ocean, even in the regions where instabilities are strong.

4. Summary and discussion

In this paper, an ocean general circulation model, HYCOM, and a linear continuously stratified ocean model are used to understand the origins and dynamics of the observed spectral peak at 90- and secondary peaks at 30–60-day periods in the equatorial Indian Ocean (Figs. 1 and 2). The model basin resembles the

realistic tropical Indian Ocean north of 30°S, and realistic solutions are found for the period of 1988–2001 when forced by 3-day mean NCEP–NCAR reanalysis fields combine with CMAP pentad precipitation. The observed intraseasonal currents and sea level in the equatorial Indian Ocean are reasonably simulated by HYCOM (Figs. 3 and 4).

The filtered 90-day SLAs from the OGCM solution and from the TOPEX data clearly show the structures of equatorial Kelvin and $l = 1$ Rossby waves (Fig. 8), which explains the spatial structure of the observed 90-day SLAs that shows a single maximum near the equator in the eastern basin (structure of equatorial Kelvin waves) and double maxima near 4° to 5° off the equator in the central basin (structure of $l = 1$ Rossby waves). These SLAs, together with HYCOM surface currents, reverse signs when the 90-day winds reverse (Fig. 8), suggesting that the observed 90-day oscillation results from the equatorial Kelvin and Rossby waves forced by the 90-day winds.

While the oceanic response peaks at 90 days, and the 90-day spectral peak dominates smaller peaks at 30–60-day periods (Figs. 1, 6, and 7), the maximum variance of winds occurs at the 30–60-day periods (Fig. 6a). This shift of peak frequency between the forcing and response indicates that the equatorial Indian Ocean selectively responds to the 90-day winds. The dominance of the 90-day peak appears not only at the surface but also in the deeper layers (Figs. 6b–d), and the 90-day variance maxima appear to move progressively westward with the increase of depth.

A hierarchy of linear model experiments with both realistic and idealized wind forcing demonstrates that the selective response of the equatorial Indian Ocean to the 90-day winds results primarily from the resonance excitation of the second baroclinic mode at the 90-day period [section 3c(2)ii]. When resonance occurs, Rossby waves reflected from the eastern ocean boundary have a large response at the 90-day period, and they act to enhance the directly forced response in the ocean interior (Figs. 10 and 11a–c). Additionally, the preferential excitation of low order and intermediate mode Kelvin and Rossby waves at lower frequencies, and the increased amplitude of high-order mode response at longer periods both contribute to the larger variance near 90 days than that near 30–60 days. The equatorial Kelvin and Rossby waves associated with the low-order and intermediate baroclinic modes are more efficiently excited near the 90-day period than at 30–60 days (dotted curves in Fig. 11b). This is because at lower frequency, both Kelvin and Rossby waves have longer wavelengths, which are more efficiently excited by the large-scale winds [section 3c(2)iii]. For the high-order baroclinic modes, Rossby waves are not available for $T \leq 90$ days [section 3c(2)iv; Fig. 12]. Therefore, responses of these modes result entirely from the directly forced Kelvin waves because no Rossby waves are available for the eastern boundary reflection (Fig. 11f). For these modes, friction acts strongly on them and pressure gradient force cannot be set up. Consequently, their responses are local to the winds. Current amplitudes are proportional to both wind strength and forcing period T. At longer period, currents associated with the high-order modes have larger amplitudes.

Consistent with previous studies, most energy is surface trapped. There is, however, a significant amount of energy associated with the low-order baroclinic modes (primarily modes 1 and 2) that penetrates through the pycnocline to the deeper ocean [section 3c(3); Fig. 13]. The westward shifting of the 90-day variance maxima with the increase of depth results from both directly forced response and reflected waves. For the directly forced response, Rossby waves excited by the wind maximum near 80°E produces a maximum surface current near the location of the wind maximum (Figs. 6a and 10d). Energy rays associated with the first two baroclinic mode Rossby waves propagate down via the corresponding WKB ray path (Fig. 14), which explains the westward shifting of the 90-day maxima in the directly forced solution (right panels of Fig. 10). Reflected waves, however, contribute equally to the westward migration of 90-day maxima because of constructive interference between the first and second baroclinic modes near the surface and subsurface current maxima (Figs. 14g,h).

Interestingly, results from this research indicate air–sea interaction at the 90-day period in the equatorial Indian Ocean. The 90-day spectral peak also occurs in observed SST across the equatorial Indian Ocean basin (Fig. 16). This SST peak may be a result of the selective response of the equatorial Indian Ocean to the 90-day winds. The zonal SST gradients at the equator may further feedback to the atmosphere to enhance the 90-day winds, which may explain the westward extension of 90-day wind variance in the western basin (Fig. 6a). The intensified 90-day winds may further feedback to the ocean to amplify the 90-day oceanic response [section 3c(5)]. Detailed studies on how the 90-day SST signal is generated and how the SST feedbacks to the atmosphere to affect the 90-day winds are an important part for our ongoing and future research, and are crucial to our understanding of the Indian Ocean intraseasonal variabilities and their impacts on the monsoon and ENSO.

As for the 90-day oscillation, the observed 30–60-day spectral peaks of currents and sea level in the equatorial Indian Ocean are primarily wind driven (section 3d). The secondary peaks of currents and SLAs at this period band correspond to the maximum peaks of intraseasonal winds at 30–60-day periods (Fig. 6a). At these frequencies, Rossby waves are only available for the first three baroclinic modes (Fig. 12). Consequently, the observed 30–60-day surface currents result primarily from the directly forced, local response of the high-

order modes and equatorial wave response of the low-order modes (Fig. 11). Reflected Rossby waves have visible contributions in the deeper layers, where the directly forced response of the first two baroclinic modes dominates the solution. Oceanic instabilities can have significant effects on the 30–60-day variance near the western boundary and south of Sri Lanka near 5°N, consistent with the previous studies (Fig. 17).

Acknowledgments. The author thanks Dr. J. P. McCreary for carefully reading the manuscript and providing critical comments and Drs. T. Yamagata, L. L. Fu, S.-P. Xie, and D. Halkides for their valuable suggestions on improving the manuscript. I also thank Dr. Alan Wallcraft for his numerous help on configuring the HYCOM to the tropical Indian Ocean. Appreciations also go to NOAA/CDC, the University of Hawaii Data Center, and the CSR/University of Texas for making the NCEP–NCAR reanalysis fields and CMAP precipitation, daily sea level, and TOPEX sea level available on the Internet. The author is supported by NSF OCE-0136836.

REFERENCES

Bleck, R., 2002: An oceanic general circulation model framed in hybrid isopycnic-cartesian coordinates. *Ocean Modell.,* **4,** 55–88.

Cane, M. A., and D. W. Moore, 1981: A note on low-frequency equatorial basin modes. *J. Phys. Oceanogr.,* **11,** 1578–1584.

——, and E. S. Sarachik, 1981: The response of a linear baroclinic equatorial ocean to periodic forcing. *J. Mar. Res.,* **39,** 651–693.

——, and Y. du Penhoat, 1982: The effect of islands on low-frequency equatorial motions. *J. Mar. Res.,* **40,** 937–962.

Gent, P. R., and J. R. Luyten, 1985: How much energy propagates vertically in the equatorial oceans? *J. Phys. Oceanogr.,* **15,** 997–1007.

Halliwell, G. R., 1998: Simulation of North Atlantic decadal/multidecadal winter SST anomalies driven by basin-scale atmospheric circulation anomalies. *J. Phys. Oceanogr.,* **28,** 5–21.

——, 2004: Evaluation of Vertical Coordinate and Vertical Mixing Algorithms in the HYbrid Coordinate Ocean Model (HYCOM). *Ocean Modell.,* **7,** 285–322.

Han, W., J. P. McCreary, D. L. T. Anderson, and A. J. Mariano, 1999: Dynamics of the eastward surface jets in the equatorial Indian Ocean. *J. Phys. Oceanogr.,* **29,** 2191–2209.

——, D. M. Lawrence, and P. J. Webster, 2001a: Dynamical response of equatorial Indian Ocean to intraseasonal winds: Zonal flow. *Geophys. Res. Lett.,* **28,** 4215–4218.

——, J. P. McCreary, and K. E. Kohler, 2001b: Influence of precipitation-evaporation and Bay of Bengal rivers on dynamics, thermodynamics, and mixed layer physics in the upper Indian Ocean. *J. Geophys. Res.,* **106,** 6895–6916.

——, P. J. Webster, R. Lukas, P. Hacker, and A. Hu, 2004: Impact of atmospheric intraseasonal variability in the Indian Ocean: Low-frequency rectification in equatorial surface current and transport. *J. Phys. Oceanogr.,* **34**, 1350–1372.

Howden, S., and R. Murtugudde, 2001: Effects of river inputs into the Bay of Bengal. *J. Geophys. Res.,* **106,** 19 825–19 843.

Jerlov, N. G., 1976: *Marine Optics.* Elsevier, 231 pp.

Kalnay, E., and Coauthors, 1996: The NCEP/NCAR 40-Year Reanalysis Project. *Bull. Amer. Meteor. Soc.,* **77,** 437–471.

Kindle, J. C., and J. D. Thompson, 1989: The 26- and 50-day oscillations in the western Indian Ocean: Model results. *J. Geophys. Res.,* **94,** 4721–4736.

Large, W. G., J. C. McWilliams, and S. C. Doney, 1994: Oceanic vertical mixing: A review and a model with a nonlocal boundary layer parameterization. *Rev. Geophys.,* **32,** 363–403.

——, G. Danabasoglu, S. C. Doney, and J. C. McWilliams, 1997: Sensitivity to surface forcing and boundary layer mixing in a global ocean model: Annual-mean climatology. *J. Phys. Oceanogr.,* **27,** 2418–2447.

Levitus, S., and T. P. Boyer, 1994: *Temperature*. Vol. 4, *World Ocean Atlas 1994,* NOAA Atlas NESDIS 4, 117 pp.

——, R. Burgett, and T. P. Boyer, 1994: *Salinity*. Vol. 3, *World Ocean Atlas 1994,* NOAA Atlas NESDIS 3, 99 pp.

Luyten, J. R., and D. Roemmich, 1982: Equatorial currents at semi-annual period in the Indian Ocean. *J. Phys. Oceanogr.,* **12,** 406–413.

Madden, R. A., and P. R. Julian, 1971: Detection of a 40–50 day oscillation in the zonal wind of the tropical Pacific. *J. Atmos. Sci.,* **28,** 702–708.

——, and ——, 1972: Description of global-scale circulation cells in the tropics with a 40–50 day period. *J. Atmos. Sci.,* **29,** 1109–1123.

McCreary, J. P., 1980: Modeling wind-driven ocean circulation. Hawaii Institute of Geophysics Tech. Rep. HIG-80-3, 64 pp.

——, 1981: A linear stratified ocean model of the coastal undercurrent. *Philos. Trans. Roy. Soc. London,* **302A,** 385–413.

——, W. Han, D. Shankar, and S. R. Shetye, 1996: On the dynamics of the East India Coastal Current, Part 2: Numerical solutions. *J. Geophys. Res.,* **101,** 113 993–114 010.

McPhaden, M. J., 1982: Variability in the central equatorial Indian Ocean. Part 1: Ocean dynamics. *J. Mar. Res.,* **40,** 157–176.

——, J. A. Proehl, and L. M. Rothstein, 1986: The interaction of equatorial Kelvin waves with realistically sheared zonal currents. *J. Phys. Oceanogr.,* **16,** 1499–1515.

——, ——, and ——, 1987: On the structure of low-frequency equatorial waves. *J. Phys. Oceanogr.,* **17,** 1555–1559.

Mertz, G. L., and L. A. Mysak, 1984: Evidence for a 40–60 day oscillation over the western Indian Ocean during 1976 and 1979. *Mon. Wea. Rev.,* **112,** 383–386.

Miyama, T., J. McCreary, T. Jensen, J. Loschnigg, S. Godfrey, and A. Ishida, 2003: Structure and dynamics of the Indian-Ocean cross-equatorial cell. *Deep-Sea Res.,* **50B,** 2023–2047.

Moore, D. W., and J. P. McCreary, 1990: Excitation of intermediate-frequency equatorial waves at a western ocean boundary: With application to observations from the Indian Ocean. *J. Geophys. Res.,* **95,** 5219–5231.

Philander, S. G. H., 1978: Forced oceanic waves. *Rev. Geophys. Space Phys.,* **16** (1), 15–46.

——, and R. C. Pacanowski, 1980: The generation of equatorial currents. *J. Geophys. Res.,* **85,** 1123–1136.

——, and ——, 1981: Response of equatorial oceans to periodic forcing. *J. Geophys. Res.,* **86** (C3), 1903–1916.

Qiu, B., M. Mao, and Y. Kashino, 1999: Intraseasonal variability in the Indo–Pacific Throughflow and the regions surrounding the Indonesian Seas. *J. Phys. Oceanogr.,* **29,** 1599–1618.

Reppin, J., F. A. Schott, J. Fischer, and D. Quadfasel, 1999: Equatorial currents and transports in the upper central Indian Ocean: Annual cycle and interannual variability. *J. Geophys. Res.,* **104,** 15 495–15 514.

Reynolds, R., and T. Smith, 1994: Improved global sea surface temperature analyses. *J. Climate,* **7,** 929–948.

Rothstein, L. M., D. W. Moore, and J. P. McCreary, 1985: Interior reflections of a periodically forced equatorial Kelvin wave. *J. Phys. Oceanogr.,* **15,** 985–996.

Schott, F., and J. P. McCreary, 2001: The monsoon circulation of the Indian Ocean. *Progress in Oceanography,* Vol. 51, Pergamon, 1–123.

Schouten, M. W., W. P. M. de Ruijter, P. J. van Leeuwen, and H. A. Dijkstra, 2002: An oceanic teleconnection between the

equatorial and southern Indian Ocean. *Geophys. Res. Lett.,* **29,** 1812, doi:10.1029/2001GL014542.

Sengupta, D., R. Senan, and B. N. Goswami, 2001: Origin of intraseasonal variability of circulation in the tropical central Indian Ocean. *Geophys. Res. Lett.,* **28,** 1267–1270.

Shankar, D., J. P. McCreary, W. Han, and S. R. Shetye, 1996: On the dynamics of the East India Coastal Current, Part 1: Analytic solutions forced by interior Ekman pumping and local alongshore winds. *J. Geophys. Res.,* **101** (C6), 13 975–13 991.

Waliser, D. E., R. Murtugudde, and L. E. Lucas, 2003: Indo-Pacific Ocean response to atmospheric intraseasonal variability: 1. Austral summer and the Madden-Julian Oscillation. *J. Geophys. Res.,* **108,** 3160, doi:10.1029/2002JC001620.

Woodbury, K. E., M. E. Luther, and J. J. O'Brien, 1989: The wind-driven seasonal circulation in the southern tropical Indian Ocean. *J. Geophys. Res.,* **94,** 17 985–18 002.

Xie, P., and P. A. Arkin, 1996: Analyses of global monthly precipitation using gauge observations, satellite estimates, and numerical model predictions. *J. Climate,* **9,** 840–858.

Yoon, J.-H., 1981: Effects of islands on equatorial waves. *J. Geophys. Res.,* **86,** 10 913–10 920.